https://doi.org/10.5194/egusphere-2026-4322
Preprint. Discussion started: 17 August 2026

A multi-model analysis of the transatlantic dust transport, deposition, and optical properties in the AeroCom Phase III

Jianyu Zheng[1,2], Hongbin Yu[2], Chamara Rajapakse[2,3], Mian Chin[1,2], Michael Schulz[4], Yves Balkanski[5], Susanne E. Bauer[6], Huisheng Bian[1,2], Peter Colarco[2], Dongchul Kim[1,2], Ramiro Checa-Garcia[5], Yevgeny Derimian[7], Oleg Dubovik[7], Paul Ginoux[8], Zak Kipling[9], Jasper F. Kok[10], Harri Kokkola[11,12], Philippe Le Sager[13], Lei Li[14], Marianne Tronstad Lund[15], Gunnar Myhre[15], Hitoshi Matsui[16], Dirk J. L. Olivie[4], Samuel Remy[17], Oyvind Seland[4], Qianqian Song[1], Toshihiko Takemura[18], Qian Tan[19,20], Kostas Tsigaridis[6,21], Twan van Noije[12], David Winker[22], Bin Xie[23], Hua Zhang[23], Xindan Zhang[14], Zhibo Zhang[1]

1. GESTAR-II, University of Maryland at Baltimore County, Baltimore, Maryland, USA
2. Earth Sciences Division, NASA Goddard Space Flight Center, Greenbelt, Maryland, USA
3. Science Systems and Application Inc., Lanham, Maryland, USA
4. Norwegian Meteorological Institute, Oslo, Norway
5. Laboratoire des Sciences du Climat et de l'Environnement, LSCE/IPSL, CEA-CNRS-UVSQ, UPSaclay, Gif-sur-Yvette, France
6. NASA Goddard Institute for Space Studies New York City, New York, USA
7. Laboratoire d'optique Atmosphèrique (LOA), Universite Lille, Villeneuve d ascq, France
8. NOAA Geophysical Fluid Dynamics Laboratory, Princeton, New Jersey, USA
9. European Centre for Medium-Range Weather Forecasts, Reading, UK
10. University of California Los Angeles, Los Angeles, California, USA
11. Department of Technical Physics, University of Eastern Finland, Kuopio, Finland
12. Atmospheric Research Centre of Eastern Finland, Finnish Meteorological Institute, Kuopio, Finland
13. Royal Netherlands Meteorological Institute, De Bilt, the Netherlands
14. Department of Atmospheric and Oceanic Sciences & Institute of Atmospheric Sciences, Fudan University, Shanghai, China
15. CICERO Center for International Climate Research, Oslo, Norway
16. Institute for Space–Earth Environmental Research, Nagoya University, Nagoya, Japan
17. HYGEOS, Lille, France
18. Research Institute for Applied Mechanics, Kyushu University, 6-1 Kasuga-koen, Kasuga, Fukuoka, Japan
19. Bay Area Environmental Research Institute, Moffett Field, California, USA
20. NASA Ames Research Center, Moffett Field, California, USA
21. Center for Climate Systems Research, Columbia University, New York City, NY, USA
22. NASA Langley Research Center, Hampton, Virginia, USA
23. Chinese Academy of Meteorological Sciences, Beijing, China

* Correspondence: Jianyu Zheng (jzheng3@umbc.edu)

Abstract

Transatlantic dust from North Africa is the largest intercontinental aerosol flux on Earth, affecting radiative forcing, cloud processes, and biogeochemical cycling, yet the inter-model spread of dust transport remains large in previous AeroCom experiments. With the progress in 17 AeroCom Phase III (P3) models, this study evaluates the transatlantic dust cycle for 2010 against AERONET inversions, satellite products (MODIS, CALIOP, MISR, IASI, POLDER, and MODIS-TIR), DustCOMM, CAMS, MERRA-2, in-situ records, and GPCP precipitation across subregions from North Africa to the Caribbean. We found that AeroCom P3 narrows mid-visible dust optical depth (DOD) diversity to 30–45% across the transport domain relative to AeroCom P2 (38–59%), yet this convergence masks compensatory biases, as models with lower (or higher) mass loading may

https://doi.org/10.5194/egusphere-2026-4322
Preprint. Discussion started: 17 August 2026

have higher (or lower) mass extinction efficiency (MEE), yielding similar DOD despite a large spread of mass representations. Compared with observational estimates, model biases intensify with transport distance, with median DOD underestimated by ~50% and ~70% over mid- and long-range regions, and loss frequencies exceed satellite estimates by a factor of 2–3. Such biases remain unresolved even with super-coarse extensions, indicating that constraining mid-visible DOD alone is inadequate for the dust cycle. The excess removal implicates deficiencies in gravitational settling, wet scavenging, and vertical transport parameterizations. This systematic underestimation could propagate into dust radiative forcing, cloud-dust interactions, and nutrient delivery to Atlantic and Amazonian ecosystems. Progress requires size-resolved benchmarking (DOD at 550 nm and 10 μm with size-segregated mass), non-spherical settling treatments, and mechanisms sustaining coarse particles aloft.

1. Introduction

The transatlantic transport of mineral dust (referred to as "dust" hereafter) from North Africa to the Americas represents the largest intercontinental aerosol flux on Earth (Yu et al., 2015a; Proestakis et al., 2025). Each year, hundreds of teragrams of dust are emitted from the Sahara Desert and Sahel region and carried westward across more than 8,000 kilometers of ocean, with pronounced seasonal and interannual variability driven by the West African monsoon system, the Saharan Air Layer, and the Intertropical Convergence Zone. This dust transport affects the Earth system along its transit pathway. Through interactions with both solar and thermal infrared radiation (Di Biagio et al., 2020; Osborne et al., 2011), transatlantic dust modulates the radiation budget over a vast oceanic domain, with important consequences for sea surface temperatures and Atlantic hurricane activity (Evan et al., 2006; Zhang et al., 2007). Dust particles serve as cloud condensation nuclei and ice nuclei, modifying cloud properties and precipitation processes over the tropical Atlantic (Karydis et al., 2011). The deposition of nutrient-rich dust, particularly iron and phosphorus, fertilizes marine ecosystems across the Atlantic and sustains terrestrial productivity in the Amazon basin (Yu et al., 2015b; Westberry et al., 2022), with broader implications for the global carbon cycle (Maher et al., 2010). Additionally, transatlantic dust degrades air quality in Caribbean and American coastal populations, contributing to respiratory health burdens (Yang et al., 2022). Given the breadth and magnitude of these impacts, a thorough understanding of transatlantic dust transport including emission, atmospheric transit, and deposition, is essential for assessing and mitigating these effects.

Global aerosol models are the primary tools for simulating the dust cycle, yet accurately representing the various dust properties (e.g., size distribution, shape, and mineral composition) remains challenging and highly uncertain (Kok et al., 2023; Gonçalves Ageitos et al., 2023). The Aerosol Comparisons between Observations and Models (AeroCom) project, an open international initiative launched in the early 2000s, has systematically advanced model evaluation through coordinated multi-model experiments. In AeroCom Phase I (P1), Huneeus et al. (2011) evaluated 15 global models and revealed inter-model differences of a factor of 2 in dust optical depth (DOD) and a factor of 10 in dust emissions, with models particularly struggling to simulate dust transport to downwind oceanic regions. Subsequent AeroCom Phase II (P2) experiments for transatlantic dust (Kim et al., 2014) and trans-Pacific Asian dust (Kim et al., 2019) are evaluated against multi-satellite observations. Both studies found that most models underestimate DOD downwind of the source and attributed the inter-model DOD diversity to compensating biases among dust emissions, residence time, and mass extinction efficiency. Recently, the AeroCom Phase III (P3) control

https://doi.org/10.5194/egusphere-2026-4322
Preprint. Discussion started: 17 August 2026

(CTRL) experiment has enrolled 17 state-of-the-science models for global aerosol simulations (Gliß et al., 2021), yet a detailed evaluation of their performance specifically for transatlantic dust transport and deposition has not been undertaken.

Satellite remote sensing has been central to characterizing transatlantic dust transport. Multiple instruments now provide complementary constraints on dust properties across the transport corridor: the Moderate Resolution Imaging Spectroradiometer (MODIS) retrieves dust optical depth (DOD) over both land and ocean using visible-to-near-infrared spectra (Kaufman et al., 2005; Yu et al., 2009, 2020; Pu and Ginoux, 2018; Zheng et al., 2026); the Multi-angle Imaging SpectroRadiometer (MISR) discriminates dust from other aerosols using multi-angle observations (Kahn and Gaitley, 2015); the Cloud-Aerosol Lidar with Orthogonal Polarization (CALIOP) provides vertically resolved dust extinction profiles based on depolarization ratio measurements (Yu et al., 2015a; Song et al., 2021); and thermal infrared sensors such as the Infrared Atmospheric Sounding Interferometer (IASI) and MODIS thermal infrared channels are particularly sensitive to coarse-mode dust particles (Zheng et al., 2023, 2026). Yu et al. (2019) demonstrated the power of a multi-sensor approach by combining CALIOP, MODIS, MISR, and IASI to estimate dust deposition along transatlantic transit routes on a seasonal basis. Together, these satellite datasets form a multi-platform observational framework for evaluating model simulations of dust transport from North Africa to the Americas.

In this study, we present a comprehensive evaluation of transatlantic dust simulations in 2010 from 17 AeroCom P3 models, using a multi-platform observational framework that includes a range of in-situ and remote sensing observational datasets. Our objectives are twofold. First, we assess model performance across the full suite of dust cycle variables, including emissions, DOD, mass loading, mass extinction efficiency, vertical profiles, deposition flux, loss frequency, near-surface mass concentration, and precipitation rate, across four transatlantic subregions North Africa (NAF), East Atlantic Ocean (EAO), Caribbean region (CAR), and Gulf of Guinea (GOG), as illustrated in Figure 1. Second, by analyzing model biases relative to this multi-parameter observational database, we diagnose specific process deficiencies responsible for inter-model divergences and identify priorities for improving transatlantic dust simulations. The remainder of this paper is organized as follows: Section 2 describes the models and observational datasets, Section 3 presents the results of model-observation comparisons, Section 4 discusses the implications, and Section 5 summarizes the main conclusions.

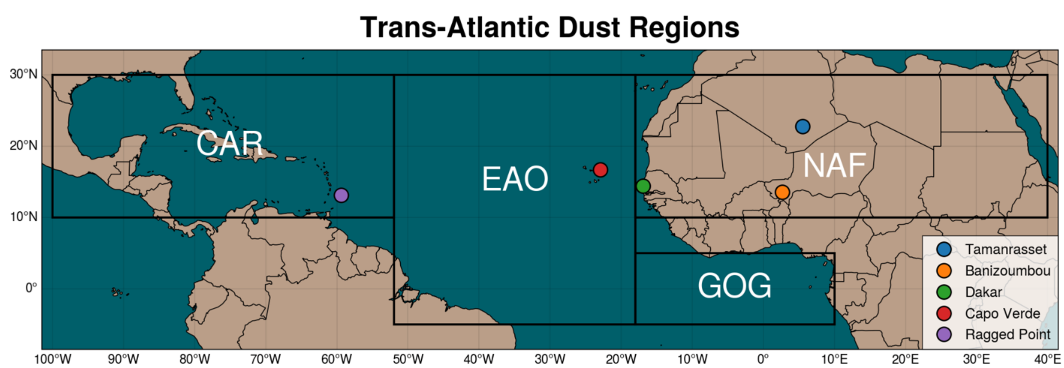

Figure 1: The latitude and longitude range of the defined subregions over the transatlantic region: North Africa

https://doi.org/10.5194/egusphere-2026-4322
Preprint. Discussion started: 17 August 2026

(NAF), East Atlantic Ocean (EAO), Caribbean region (CAR), and Gulf of Guinea (GOG). Colored circles indicate the five selected AERONET sites dominated by dust within the transatlantic region: Tamanrasset, Banizoumbou, Dakar, Capo Verde, and Ragged Point.

2. Descriptions of models and data

2.1. AeroCom models

In this study, the 17 global aerosol transport models participating in the AeroCom P3 Control experiment (CTRL) ran dust cycle simulations with meteorology in 2010. The major features of the models are summarized in Table 1, with references therein for additional information on the models. The spatial resolutions among models span from 0.352 degrees to 3 by 2 degrees.

Dust particle size distributions and cut-off size have diverse settings among the models. While 7 models parameterize the dust size distributions with 1, 2, or 4 modes, the other models treat dust with 3-12 bins with different resolutions. The cut-off sizes for dust differ among the models and we broadly categorize the models into two groups with an upper limit size range at about 15 µm (group 1) or 40 µm (group 2) in diameter (D). In particular, two models' dust transport simulations, ECMWF-CY46 and INCA-4DU, have enhanced the contribution of super-coarse dust particles (D > 20 µm) compared with their previous versions (ECMWF-CY45 and INCA), which are categorized as Group 3. They handle these large particles differently in their approach. Specifically, ECMWF-CY46 retains the same three size bins as CY45 (Rémy et al., 2022; Rémy et al., 2019) but redistributes the emitted mass among bins with nearly all emitted mass (98.45%) toward the largest size bin compared to CY45 (see Table 1). INCA-4DU extends the emitted size distribution to four lognormal modes spanning 0.1–400 µm, compared to INCA, which employs a single moderate size mode (Table 1). The inclusion of the two large size modes enables INCA-4DU to represent a population of super-coarse and giant particles that is absent in the standard INCA configuration. These updates provide a direct opportunity to evaluate whether enhanced super-coarse dust representations that were documented as a significant underestimation in previous model results (Adebiyi and Kok, 2020; Meng et al., 2022; Drakaki et al., 2022), can improve the simulation of transatlantic dust transport (details in Section 3.7).

Not all models provide outcomes for the full list of dust properties. For example, GISS-MATRIX uses an aerosol microphysical scheme with internal mixture among aerosol species, which does not provide aerosol optical depth (AOD) for a specific component, such as dust. BCC-CUACE provides mass-related variables but not optical depth and extinction profiles. The transatlantic domain average of available dust properties in each model are listed in Table S1. As the models originally have different spatial resolutions, we first harmonized outputs of individual models at their native grid systems to that over the same 1° × 1° resolution. At each grid cell, we sorted through the variables from all models and then calculated their median, which is more suitable than the multi-model mean in terms of minimizing potential biases being introduced by extreme values from some models. Here, the two models in Group 3 are excluded from the multi-model median calculation, as they will be evaluated with their predecessors for presenting the effects of including super-coarse particles in Section 3.7.

https://doi.org/10.5194/egusphere-2026-4322
Preprint. Discussion started: 17 August 2026

178 **Table 1: Description of the AeroCom Phase III models considered in this study.**

Size Group	Model	Resolution (lon x lat) (layers (<10km))	Dust Emission	Dust size distribution (Diameter)	Meteorology	Major References
Group 1	CAM5-ATRAS	2.5° x 1.875° 30 (15)	Modified DEAD model (Zender et al., 2003; Kok et al., 2014)	12 bins 0.001 - 10 µm	MERRA-2	Matsui (2017); Matsui and Mahowald (2017)
	EC-Earth3-AerChem	3° x 2° 34	Modified Tegen et al. (2002)	2 modes 0.1–1 µm, 1–16 µm; sigma=1.59, 2.0	IFS-based GCM nudged to ERA-Interim	Van Noije et al. (2021)
	ECHAM-HAM	1.875° x 1.875° 47 (19)	Modified Tegen et al. (2002) (Cheng et al., 2008; Heinold et al., 2009)	Same as EC-Earth3-AerChem	ERA-Interim	Tegen et al. (2019)
	ECHAM-SALSA (echam6.1.0-ham2.1-moz0.8)	1.875° x 1.875° 47 (19)	same as ECHAM-HAM	7 bins 0.05 - 10 µm	ERA-Interim	Kokkola et al. (2018)
	INCA	2.5° x 1.26° 79 (39)	Balkanski et al. (2008)	1 mode MMD=2.5 µm; sigma=2.0 at emission	ERA-Interim	Huneeus et al. (2011); Checa-Garcia et al. (2021)
	NorESM2	1.25° x 0.94° 32 (15)	Zender et al. (2003)	2 modes MMD=0.44, 1.26 um; sigma = 1.59, 2.0	ERA-Interim	Kirkevåg et al. (2018)
	TM5	3° x 2° 34	same as EC-Earth3-AerChem	Same as EC-Earth3-AerChem	ERA-Interim	Van Noije et al. (2021)
Group 2	BCC-CUACE	2.813° x 2.813° 26	Gong et al. (2003), Zhou et al. (2012)	12 bins 0.005 - 20.48 µm	BCC-GCM (interacted with aerosol changes)	Zhao et al. (2015); Zhang et al. (2016)
	ECMWF-CY45	0.352° x 0.352° 60 (28)	Ginoux et al. (2001)	3 bins 0.06-1.1-1.8-40 µm	ECMWF-IFS	Rémy et al. (2019)
	GEOS	1.0° x 1.0° 72 (28)	Ginoux et al. (2001), Kim et al. (2013)	5 bins 0.2-2.0-3.6-6-12-20 µm	MERRA-2	Colarco et al. (2010); Chin et al. (2002)
	GFDL-AM4	1.25° x 1.0° 33 (19)	Ginoux et al. (2001)	Same as GEOS	NCEP-NCAR reanalysis	Zhao et al. (2018)
	GISS-MATRIX	2.5° x 2.0° 40 (18)	Cakmur et al. (2006), Miller et al. (2006)	6 bins 0.2-1-2-4-8-16-32 µm	NCEP-NCAR reanalysis	Bauer et al. (2020); Bauer et al. (2008)
	GISS-OMA	2.5° x 2.0° 40 (18)	Cakmur et al. (2006), Miller et al. (2006)	Same as GISS-MATRIX	NCEP-NCAR reanalysis	Bauer et al. (2020)
	OsloCTM3	2.25° x 2.25° 60 (28)	DEAD (Zender et al. 2003)	8 bins 0.03–0.07–0.16–0.37–0.87–2.01–4.65–10.79–25 µm	ECMWF-openIFS	Grini et al. (2005); Lund et al. (2018)
	SPRINTARS	0.563° x 0.563° 40 (21)	Gillette (1978), Takemura et al. (2009)	6 bins 0.2-0.44-0.92-2.0-4.3-9.28-20 µm	ERA-Interim	Takemura et al. (2003)
Group 3 (enhance super-coarse particles)	ECMWF-CY46	0.352° x 0.352° 137 (58)	Saltation: Marticorena and Bergametti (1995) Emission size: Kok et al. (2011)	3 bins same as in ECMWF-CY45, with mass ratio at emission as 0.15%, 1.4%, 98.45%	ECMWF-IFS	Rémy et al. (2022)
	INCA-4DU	2.5° x 1.26° 79 (39)	same as INCA	4 modes 0.1- 400 µm with MMD (sigma) = 1 (1.8), 2.5 (2.0), 7 (1.9), and 22 (2.0)	ERA-Interim	Huneeus et al. (2011); Checa-Garcia et al. (2021)

https://doi.org/10.5194/egusphere-2026-4322
Preprint. Discussion started: 17 August 2026

To obtain the basic statistics of models, we calculate the multi-model mean, median and diversity for each variable from the available models in each grid box, which is listed in Table S2 in the supplementary. The diversity is defined as the standard deviation divided by the multi-model mean for each variable among the available models in each grid box (Textor et al., 2006), which is equivalent to the coefficient of variation. However, we retain the term 'diversity' in this study for consistency with previous AeroCom experiments (Textor et al., 2006; Huneeus et al., 2011; Kim et al., 2014; Gliß et al., 2021).

2.2. Observations and observation-constrained characterization of dust

To evaluate the transatlantic dust simulations from multiple global aerosol transport models (Section 2.1), we obtain six satellite retrieval products, the observationally constrained DustCOMM dataset and MERRA-2 and CAMS reanalysis-based products, 125 climatological in-situ deposition measurements, long-term AERONET and surface dust concentration records, and global precipitation observations, which are listed in Table 2. A brief description of these observational datasets is provided in the supplementary Sections S1-S4.

Table 2: Observational and reanalysis-based datasets used in this study to evaluate the transatlantic dust transport

Variables	Sources	Major references
Dust optical depth (mid-visible)	MODIS	Yu et al. (2009); Yu et al. (2020); Pu and Ginoux (2018)
	MISR	Kahn and Gaitley (2015); Garay et al. (2020)
	CALIOP	Yu et al. (2015a)
	MODIS-TIR	Zheng et al. (2023); Zheng et al. (2026)
	IASI-LMD	Capelle et al. (2018)
	POLDER	Li et al. (2022)
	AERONET	Dubovik et al. (2006)
	MERRA-2	Gelaro et al. (2017)
	CAMS	Inness et al. (2019)
	DustCOMM	Kok et al. (2021)
Dust mass loading (coarse)	MODIS-TIR	Zheng et al. (2023); Zheng et al. (2026)
	POLDER	Li et al. (2022)
	AERONET	Zhang et al. (2024)
	MERRA-2	Gelaro et al. (2017)
	CAMS	Inness et al. (2019)
	DustCOMM	Kok et al. (2021)

https://doi.org/10.5194/egusphere-2026-4322
Preprint. Discussion started: 17 August 2026

Dust concentration (near-surface)	In-situ measurements in Barbados and Miami	Zuidema et al. (2019)
Dust extinction coefficient (profile)	CALIOP	Yu et al. (2015a), Song et al. (2021)
Dust deposition	In-situ sediment traps	Albani et al. (2014), Friese et al. (2017); Korte et al. (2017)
	Satellite-based estimation	Yu et al. (2019)
	DustCOMM	Kok et al. (2021)
Dust loss frequency	Satellite-based estimation	Yu et al. (2019)
Precipitation rate at surface	GPCP	Adler et al. (2018)

3. Results

This section presents model-observation discrepancies and comparisons with in-situ measurements for dust emissions (Section 3.1), optical depth and mass loading (Section 3.2), vertical distributions (Section 3.3), deposition and loss frequency (Section 3.4), surface mass concentrations (Section 3.5), precipitation rate (Section 3.6), and super-coarse dust evolution (Section 3.7) across four selected transatlantic subregions (Figure 1). To make it concise, we only present spatial distributions of the multi-model median and inter-model diversity for each variable and compare these with satellite products. Spatial variations of each variable for individual models are included in the supplementary materials.

3.1 Dust emissions

Figure 2a shows that dust emission in the NAF source region exhibits approximately twofold spread over major "hot-spot" dust sources (diversity ~50%) to 2–4 times greater diversity in Sahel and coastal regions (diversity 100%–200%) among the P3 models, with the median value of 110 mg m^{-2} day^{-1} (Figure 2b and 2e) (corresponding to ~539 Tg yr^{-1} over the domain), which is typically due to the different settings of the dust emission scheme and dust source map (see Figure S1). The different dust source maps and emission parameterization lead to different dust emission fluxes, even with the same meteorological conditions, such as surface wind speed.

The model median dust emission in NAF is similar to that of DustCOMM PM10 (Figure 2e). By comparing the domain average of NAF dust emission from AeroCom models Group 1 and Group 2 in Figure 2g, we found unsubstantial differences, suggesting that extending the particle size range to 20 μm contributes minimally to total emissions in these models. Yet, the substantial increase observed between DustCOMM PM10 and PM20 (Figures 2e and 2f) indicates that the 10–20 μm size fraction should, in principle, account for a considerable portion of dust emission flux (Kok et al., 2017). We also found that the dust emission in DustCOMM PM20 exceeds all AeroCom Group 2 models, as shown in Figure 2g, likely stemming from differences in how particle size distributions (PSD), especially fresh-emitted PSD, are parameterized at the source, and what the amount of global total dust emission is targeted.

https://doi.org/10.5194/egusphere-2026-4322
Preprint. Discussion started: 17 August 2026

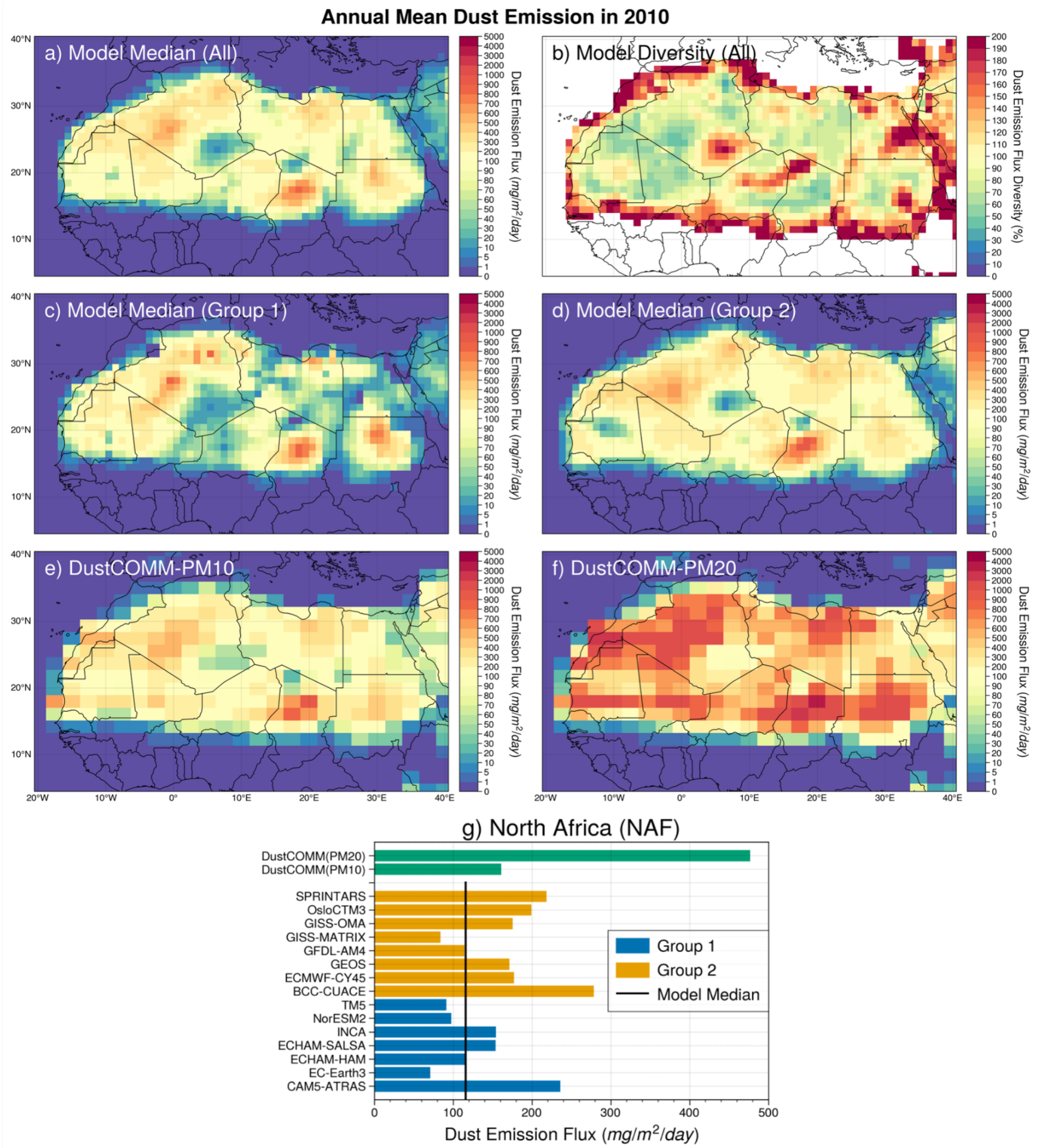

Figure 2: Annual mean dust emission flux over North Africa for 2010. (a) Model median and (b) Model diversity (standard deviation/mean, expressed as a percentage) of emission flux (mg m^{-2} day^{-1}) across the P3 ensemble. (c, d) Model median emission flux (mg m^{-2} day^{-1}) for Group 1 and Group 2 models. (e, f) DustCOMM emission flux estimates for PM10 and PM20, respectively. (g) Bar chart of area-averaged dust emission flux (mg m^{-2} day^{-1}) over the NAF domain for individual models and DustCOMM products. Blue and orange bars denote Group 1 and Group 2 model simulations, respectively. The model median is represented by the black vertical lines.

3.2 Dust optical depth, mass extinction efficiency, and mass loading

Having established the emission baseline in Section 3.1, we now evaluate the atmospheric dust

https://doi.org/10.5194/egusphere-2026-4322
Preprint. Discussion started: 17 August 2026

burden in terms of DOD, which is calculated from the mass concentration and size-dependent mass extinction efficiency (MEE) in the models. This evaluation directly reflects model performance in simulating dust transport from source to receptor regions.

3.2.1 Dust optical depth

To evaluate the dust transport simulations in AeroCom P3, we first compare the seasonal cycle of DOD at 550 nm from the P3 models with AERONET coarse-mode AOD at five dust-dominated sites along the transatlantic transport pathway, as shown in Figure 3. The observed seasonal cycles differ markedly among the sites. AERONET shows a late-spring to early-summer maximum at Tamanrasset in the central Sahara, an early-spring maximum at Banizoumbou in the Sahel, a relatively weak seasonal contrast at coastal Dakar, and a pronounced summer maximum at Capo Verde and Ragged Point associated with the summertime westward dust transport across the Atlantic. The model median reproduces these seasonal cycles well (r of 0.8 to 0.97).

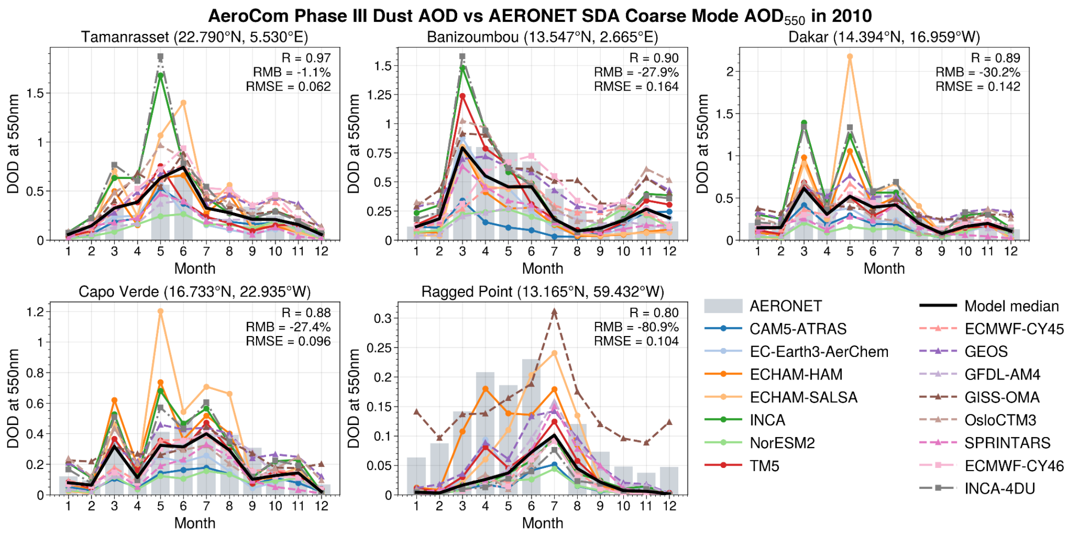

Figure 3: Seasonal cycle of DOD at 550 nm from AeroCom P3 models compared with AERONET coarse-mode AOD at five dust-dominated sites along the transatlantic corridor: (a) Tamanrasset (NAF), (b) Banizoumbou (NAF), (c) Dakar (EAO), (d) Capo Verde (EAO), and (e) Ragged Point (CAR). Group 1 (solid dot), Group 2 (dashed triangle) and Group 3 (dashed rectangle) models are shown separately. The grey bars denote AERONET observations; colored lines represent individual model simulations. The solid black lines indicate the multi-model median. Basic statistics of multi-model median compared with AEROENT are shown in the upper right of each panel.

In contrast to the well-captured seasonal variation, models DOD are progressively underestimated with transport distance. The model median agrees with AERONET within 1%–28% at the NAF source sites (Tamanrasset and Banizoumbou), underestimates by ~30% at Dakar and Capo Verde, and falls ~80% below AERONET at Ragged Point in the Caribbean, where the deficit is largest during the June to July peak season. This progressive deterioration of model–observation agreement with transport distance indicates that models remove dust too efficiently during long-range transport, which is corroborated by an independent evaluation of dust loss frequency in Section 3.4.

https://doi.org/10.5194/egusphere-2026-4322
Preprint. Discussion started: 17 August 2026

Table 3 further shows main statistics of the annual mean DOD comparisons from P3 models, MERRA-2, CAMS, and DustCOMM products against coarse AOD from the 19 AERONET stations within the transatlantic region. Note that DOD from individual models in Figure 3 spread by up to a factor of more than 10, which is also revealed by the spread of models mean bias of annual mean DOD (-64% to 37% in Table 3). Meanwhile, the differences between Group 1 models (D < ~15 μm) and Group 2/3 models (D < ~40 μm or larger) are insignificant at all five sites, indicating that extending the upper size limit alone does not substantially alter DOD at mid-visible wavelengths.

Table 3: Correlations, mean bias, and RMSE for the comparisons of 2 reanalysis products, 2 DustCOMM products, and 13 models with AERONET coarse AOD at 550 nm from 18 stations within the transatlantic region.

Category	Source	Correlations	Relative Mean Bias (%)	RMSE
Reanalysis	CAMS	0.972	-33.08	0.067
	MERRA-2	0.978	-14.18	0.034
PSD-constrained model climatology	DustCOMM - PM10	0.967	-22.96	0.05
	DustCOMM - PM20	0.968	-16.88	0.042
AP3 Group 1 models	CAM5-ATRAS	0.882	-55.37	0.114
	EC-Earth3-AerChem	0.975	-42.54	0.083
	ECHAM-HAM	0.787	-1.35	0.081
	ECHAM-SALSA	0.813	26.33	0.09
	INCA	0.923	37.14	0.095
	NorESM2	0.923	-64.14	0.127
	TM5	0.972	-18.91	0.045
AP3 Group 2 models	ECMWF-CY45	0.938	-24.98	0.059
	GEOS	0.974	8.78	0.043
	GFDL-AM4	0.916	-39.84	0.092
	GISS-OMA	0.981	-25.66	0.047
	OsloCTM3	0.951	6.08	0.048
	SPRINTARS	0.924	-47.26	0.101

We also compare the median and diversity of DOD from 13 P3 models with those from six satellite observational products, two reanalysis products, and the DustCOMM DODs (PM10 and PM20), as shown in Figure 4. Here, we calculate the satellite median and diversity in the same way as models described in Section 2.1. However, because of the lower spatial resolution of CALIOP DOD compared to other products, we obtain the satellite median and diversity in 5° × 2° by aggregating the remaining satellite products.

The model median (Figure 4c) demonstrates general agreement with that of satellites in capturing the spatial pattern of DOD across the transatlantic region, with transport gradient from NAF toward EAO, GOG, and further CAR. For context, AeroCom P1 simulations exhibited diversity within a factor of 2 (Huneeus et al., 2011), while AeroCom P2 evaluations revealed that models systematically underestimated dust transport to adjacent oceanic regions over North Africa (Kim et al., 2014). Among P3 models, a moderate model diversity (30%–45%) persists over NAF, EAO, and CAR, making progress in simulating DOD compared to AeroCom P1 (a factor of 2) and P2 (38–59%) (Huneeus et al., 2011; Kim et al., 2014). However, diversity in NAF is relatively larger, which is attributable to diverse dust emission parameterizations across NAF (see Figure 2). Detailed performance of each model and satellite products can be found in Figure S2 in the

https://doi.org/10.5194/egusphere-2026-4322
Preprint. Discussion started: 17 August 2026

supplementary materials.

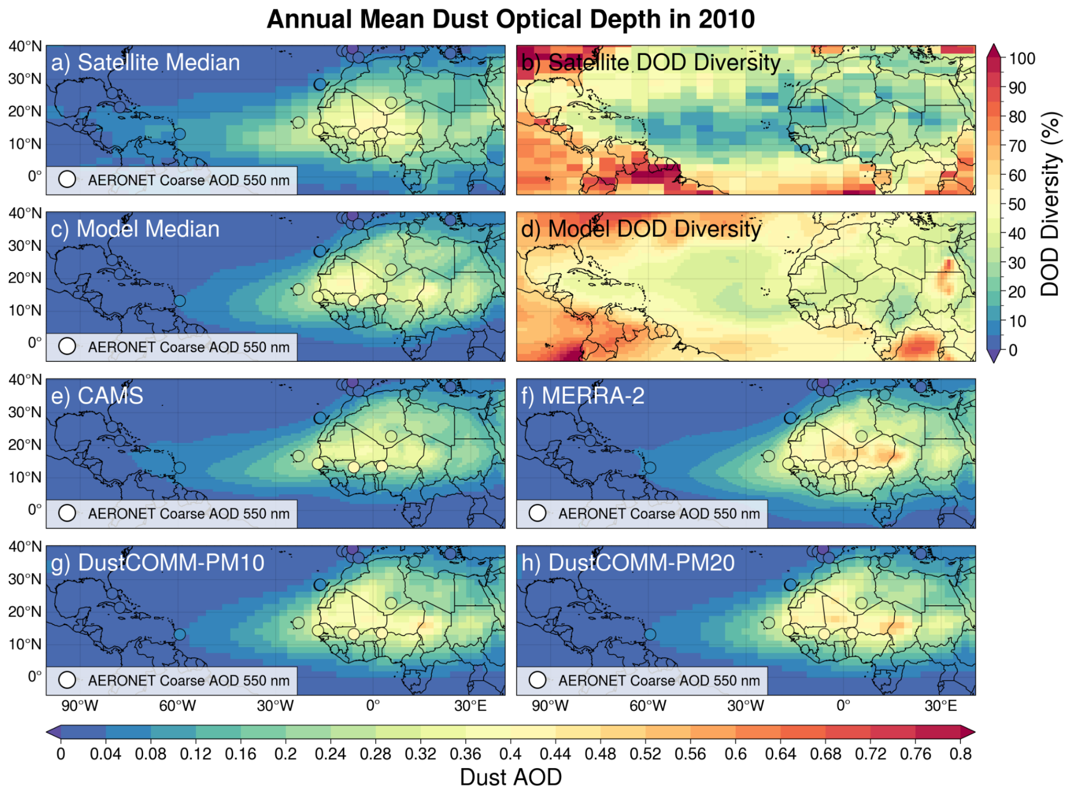

Figure 4: Annual mean dust optical depth (DOD) at 550 nm in 2010 across the transatlantic domain: (a) satellite median, (c) multi-model median, (e) CAMS reanalysis, (f) MERRA-2 reanalysis, (g) DustCOMM-PM10, and (h) DustCOMM-PM20. Panels (b) and (d) show the DOD diversity (standard deviation/mean, expressed as a percentage) for satellite products and models, respectively. Color dots in (a), (c) and (e)-(f) represent annual mean coarse-mode AOD from the 18 selected AERONET sites.

For regional DOD evaluation, Figure 5 presents domain-averaged annual mean DOD at 550 nm across four studied regions along the transatlantic pathway. Over NAF, despite considerable inter-model spread, the model median DOD (~0.25) aligns well with satellite observations (~0.27), consistent with previous findings that models adequately reproduce DOD over primary source regions (Huneeus et al., 2011). However, systematic underestimation emerges with transport distance. Both models and both DustCOMM underestimate DOD by ~50% over EAO and GOG, and by ~70% over CAR compared with satellite products. This distance-dependent bias corroborates Kim et al. (2014), who documented decay factors of 4-10 from West Africa to 60°W in AeroCom P2 models versus only a factor of 2 in satellite observations. The persistent underestimation in DustCOMM products, despite incorporating observational constraints on dust size distribution (Kok et al., 2021), suggests that the inclusion of D > 10 μm particles has little contribution to mid-visible DOD, possibly due to their relatively low mass extinction efficiency (MEE) and deficiencies in the modeled removal processes.

https://doi.org/10.5194/egusphere-2026-4322
Preprint. Discussion started: 17 August 2026

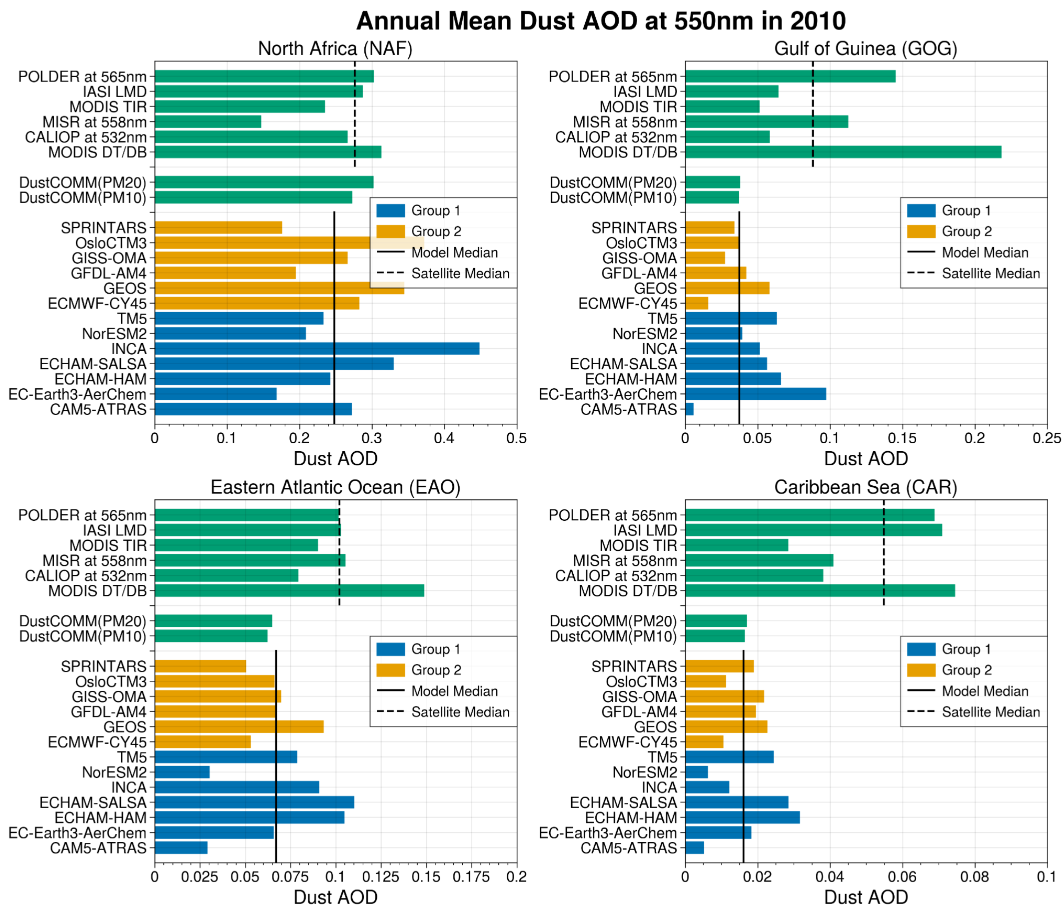

Figure 5: Annual mean DOD at 550 nm in 2010 across the four transatlantic subregions: (a) North Africa (NAF), (b) Gulf of Guinea (GOG), (c) Eastern Atlantic Ocean (EAO), and (d) Caribbean Sea (CAR). Green bars represent satellite retrievals from POLDER (565 nm), IASI, MODIS-TIR, MISR (558 nm), CALIOP (532 nm), MODIS DT/DB, and the DustCOMM estimates (PM10 and PM20). Blue and orange bars denote Group 1 and Group 2 model simulations, respectively. Solid and dashed vertical black lines indicate the model median and satellite median, respectively.

3.2.2 Dust mass loading and mass extinction efficiency

Because DOD in models is derived from simulated mass loading multiplied by the model-specific MEE, which itself depends on assumptions regarding dust properties such as particle density, size distribution, refractive index, and shape, agreement in DOD does not necessarily translate to agreement in mass loading. In this section, we evaluate the diversity of mass loading and MEE among AeroCom P3 models and assess their consistency with satellite, reanalysis, and DustCOMM products. Note that MEE in this study is referred to as the annual mean effective MEE at 550 nm as the ratio of annual mean DOD to annual mean mass loading, because instantaneous MEE values cannot be meaningfully averaged across time steps and grid cells due to their dependence on local particle size distributions.

Observational constraints of dust mass loading remain challenging to establish, as remote sensing

https://doi.org/10.5194/egusphere-2026-4322
Preprint. Discussion started: 17 August 2026

retrievals rely heavily on assumptions linking optical and microphysical properties, and direct measurements of dust mass are limited. In this section, we obtain the estimated dust mass loading from the GRASP-retrieved AERONET, POLDER, and MODIS-TIR observational data. Detailed estimation methods and introductions of data products are in the supplementary Section S5.

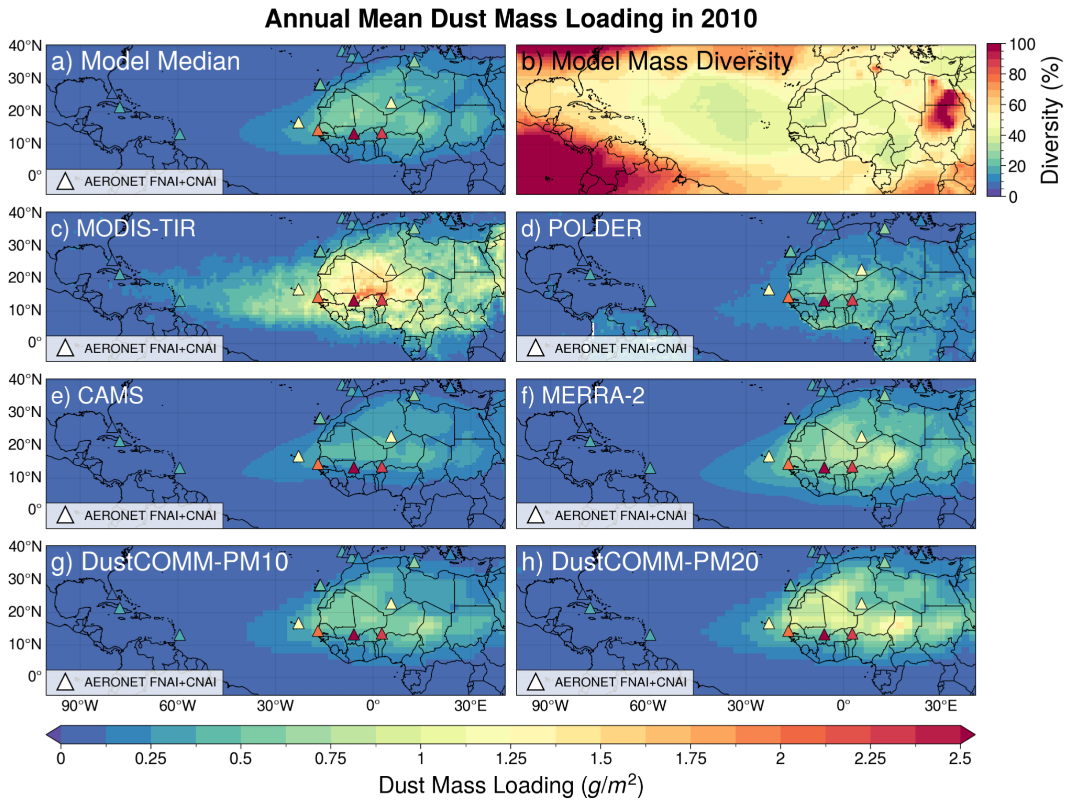

Figure 6: Annual mean dust mass loading (g m⁻²) in 2010: (a) multi-model median, (b) model mass loading diversity (standard deviation/mean, expressed as a percentage), (c) MODIS-TIR, (d) POLDER, (e) CAMS reanalysis, (f) MERRA-2 reanalysis, (g) DustCOMM-PM10, and (h) DustCOMM-PM20. Color triangles in (a) and (c)-(f) represent the AERONET FNAI+CNAI mass loading for non-absorbing dust.

Figure 6 compares the annual mean dust mass loading from the AeroCom P3 model median with the two satellite-derived products (MODIS-TIR and POLDER), CAMS and MERRA-2 reanalyses, and DustCOMM products. The AeroCom P3 ensemble exhibits similar but slightly greater diversity in mass loading compared to that of DOD (Figure 4) over NAF and EAO, with a range from 30% to 60%, except for eastern Africa, where the diversity exceeds 100%, consistent with what is observed in dust emissions while with lower diversity (see Figure 2a). This amplification of diversity from emission to loading indicates that dust removal processes, mainly dry deposition parameterizations in source regions, contribute additional sources of inter-model spread (Gliß et al., 2021). The AERONET-estimated mass loading (colored triangles in Figure 6) substantially exceeds the model median and both reanalysis and DustCOMM products at dust-dominated sites within NAF, consistent with the finding that AERONET-GRASP retrievals are approximately three times higher than MERRA-2 dust (Zhang et al., 2024).

https://doi.org/10.5194/egusphere-2026-4322
Preprint. Discussion started: 17 August 2026

As shown in both Figures 6 and 7, MODIS-TIR mass loading (~0.6–1.2 g m⁻²) also substantially exceeds the model median and most P3 models, while POLDER mass is similar to the model median and less than MERRA-2, as also reported in Li et al. (2022). These differences among observational products partly reflect the underlying retrieval assumptions. Firstly, POLDER tends to under-represent large, non-spherical mineral dust particles and thus underestimate the mass contributions from coarse particles (Formenti et al., 2018; Chen et al., 2019), while MODIS-TIR's estimates could include contributions from non-dust coarse particles (e.g., sea salts). We also note that POLDER coarse AOD at 565 nm has non-negligible differences with the derived AOD from insoluble and iron components (see Figure S5), suggesting that assuming dust as different component combinations introduces additional uncertainty.

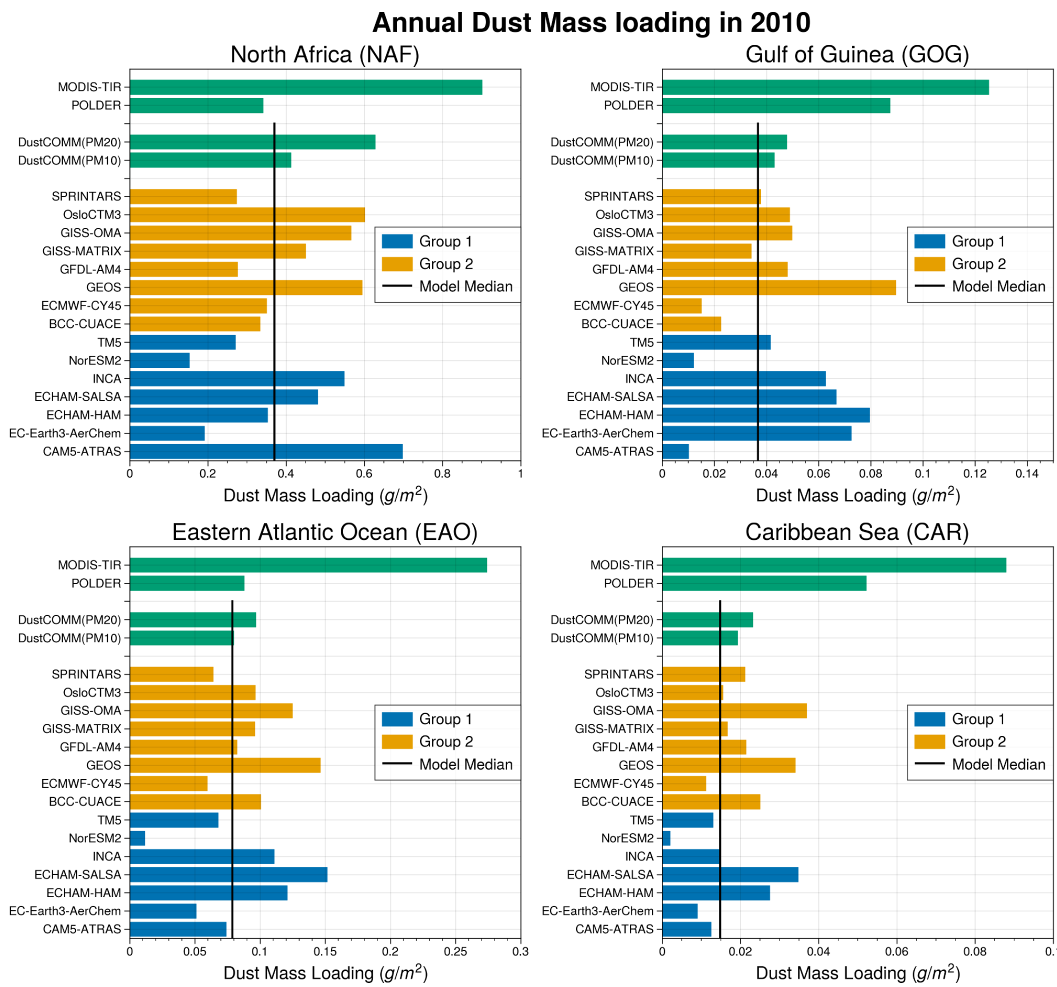

Figure 7: Annual mean dust mass loading (g m⁻²) in 2010 across the four transatlantic subregions: (a) North Africa (NAF), (b) Gulf of Guinea (GOG), (c) Eastern Atlantic Ocean (EAO), and (d) Caribbean Sea (CAR). Blue and orange bars distinguish Group 1 and Group 2 model simulations, respectively, while green bars represent the MODIS-TIR, POLDER, DustCOMM-PM10 and DustCOMM-PM20 estimates. The vertical black line indicates the multi-model median mass loading for each region.

https://doi.org/10.5194/egusphere-2026-4322
Preprint. Discussion started: 17 August 2026

Table 4 lists the statistical comparisons with AERONET-estimated dust mass loading. We found that all models give lower dust mass loading than the AERONET retrievals, with correlations ranging from 0.76 to 0.95. MODIS-TIR achieves the highest correlation (0.96), low relative difference (-39%) and RMSE (0.420) with AERONET estimates among all products. Compared with DustCOMM-PM10, DustCOMM-PM20 yields systematically higher mass loading values over NAF, yet the discrepancy with AERONET persists, reflecting the fundamental differences in assumed particle size ranges: DustCOMM-PM20 incorporates particles up to 20 µm diameter that contribute substantially to mass but relatively little to optical depth at 550 nm.

Table 4: Correlations, relative difference, and RMSE for the 2 satellite products, 2 reanalysis products, 2 DustCOMM products, and 15 models in comparison to AERONET retrievals of FNAI+CNAI mass loading at 19 stations.

Category	Source	Correlations	Relative Difference (%)	RMSE
Satellite	POLDER (Insoluble+Iron)	0.957	-82.130	0.871
	MODIS-TIR (Coarse)	0.967	-39.113	0.420
Reanalysis	CAMS	0.883	-85.015	0.908
	MERRA-2	0.965	-74.910	0.787
PSD-constrained model climatology	DustCOMM - PM10	0.949	-79.046	0.836
	DustCOMM - PM20	0.949	-71.100	0.749
AP3 Group 1 models	CAM5-ATRAS	0.773	-79.332	0.864
	EC-Earth3-AerChem	0.954	-88.826	0.937
	ECHAM-HAM	0.751	-73.885	0.837
	ECHAM-SALSA	0.784	-63.978	0.751
	INCA	0.874	-67.949	0.753
	NorESM2	0.821	-96.355	1.021
	TM5	0.947	-83.667	0.886
AP3 Group 2 models	BCC-CUACE	0.892	-77.128	0.845
	ECMWF-CY45	0.833	-83.072	0.888
	GEOS	0.947	-65.357	0.696
	GFDL-AM4	0.875	-84.649	0.913
	GISS-MATRIX	0.953	-77.302	0.801
	GISS-OMA	0.952	-71.389	0.739
	OsloCTM3	0.887	-68.365	0.748
	SPRINTARS	0.862	-85.585	0.917

The MEE comparison in Figure 8 shows considerable spread among P3 models (0.37 to 3.3 m^2 g^{-1}), with the median MEE similar to that of DustCOMM-PM10 in all four regions. POLDER MEE systematically exceeds the model median by 0.22 to 0.83 m^2 g^{-1}, while MODIS-TIR is lower than model median and DustCOMM by ~0.45 m^2 g^{-1} in all four regions. DustCOMM-PM20 MEE is approximately 10% lower than PM10, reflecting the inclusion of particles up to 20 µm that are optically insensitive at 550 nm. MEE values do not segregate systematically by particle size group, as Group 1 models do not consistently exhibit higher MEE than Group 2 models. It further suggests that other factors, such as assumptions about refractive indices, size distribution shapes, and optical calculation methods, dominate the inter-model MEE variability.

https://doi.org/10.5194/egusphere-2026-4322
Preprint. Discussion started: 17 August 2026

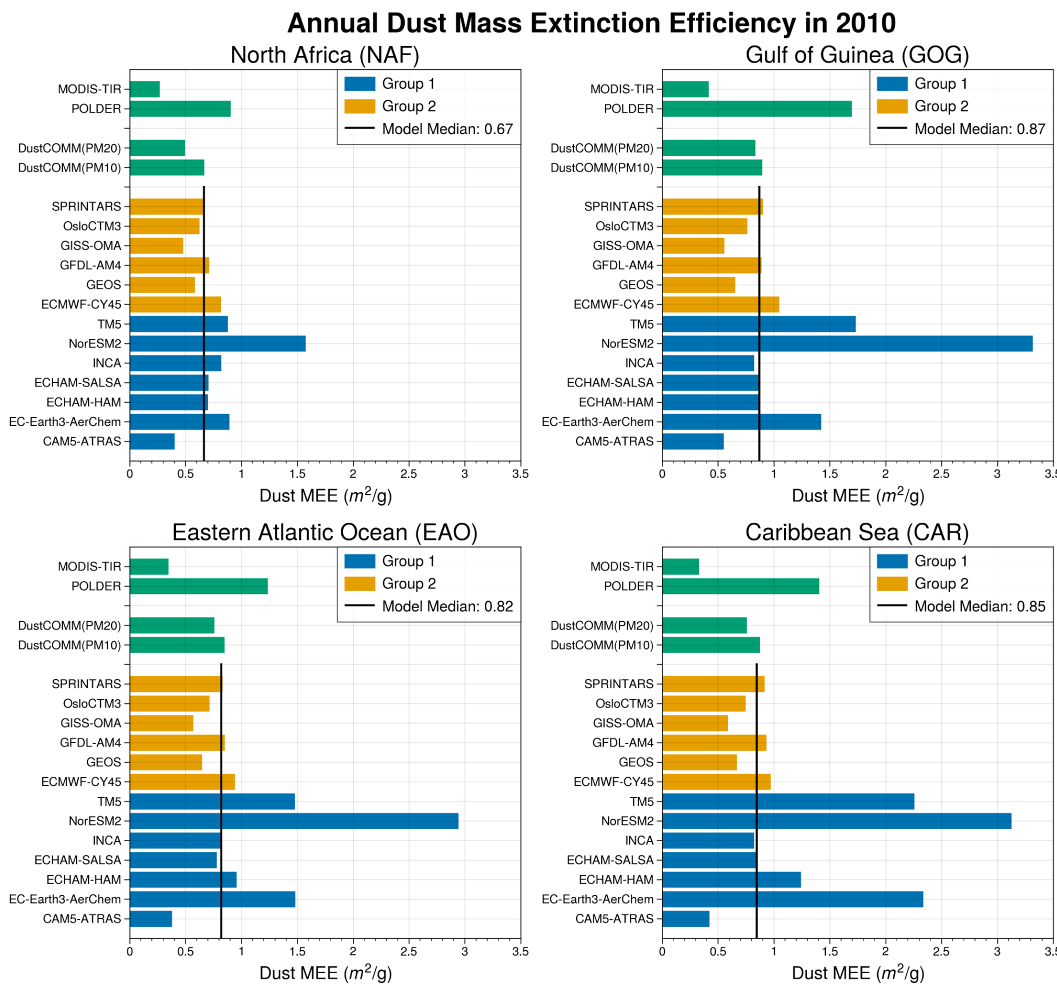

Figure 8: Annual mean dust mass extinction efficiency (MEE; m² g^{-1}) at 550 nm in 2010 across the four transatlantic subregions: (a) North Africa (NAF), (b) Gulf of Guinea (GOG), (c) Eastern Atlantic Ocean (EAO), and (d) Caribbean Sea (CAR). Blue and orange bars distinguish Group 1 and Group 2 model simulations, respectively, while green bars represent the MODIS-TIR, POLDER, DustCOMM-PM10 and DustCOMM-PM20 estimates. The vertical black line indicates the multi-model median MEE for each region.

Over NAF, the lowest MEE among P3 models (0.37 m² g^{-1}) remains 37–59% higher than that of in-situ measured dust during the Fennec campaign (0.23–0.27 m² g^{-1}), which has size distributions with effective diameters of 7–12 µm (Ryder et al., 2013a; Ryder et al., 2013b), while MODIS-TIR shows MEE from ~0.2–0.3 m² g^{-1}. Over EAO, model MEE values are similarly elevated compared to MODIS-TIR (~0.3–0.4 m² g^{-1}), and in-situ estimates from the AER-D and Fennec-SAL campaigns, which reported 0.23–0.39 m² g^{-1} for transported dust in the Saharan Air Layer (Ryder et al., 2013a; Ryder et al., 2018). Independently, Papetta et al. (2026) synthesized airborne in-situ observations and ground-based remote sensing to estimate a volume-to-extinction ratio of 1.14 µm at Cabo Verde (within EAO), corresponding to an MEE of 0.33 m² g^{-1} assuming a dust density of 2.65 g cm^{-3}, further supporting the overestimation of MEE in most AeroCom models, which is

https://doi.org/10.5194/egusphere-2026-4322
Preprint. Discussion started: 17 August 2026

possibly due to the bias-toward-finer dust size distributions.

POLDER MEE exceeds model median and MODIS-TIR by a factor of 2-3 for all four regions. Here, we should note that POLDER and MODIS-TIR MEE assumes spheroidal particles, which could yield higher MEE than spherical calculations that are used for in-situ measurements. Nonetheless, MODIS-TIR coarse-only size distribution produces lower MEE than full-size distributions. Thus, the combined effects produce MODIS-TIR MEE more consistent with what is calculated from in-situ measurements than POLDER.

The comparison among Figures 6 to 8 (also see model-specific results in Figures S3 and S4) reveals that the apparent consistency in DOD among models (Figure 4) arises partly from compensatory settings: models with lower (higher) mass loading tend to exhibit higher (lower) MEE corresponding to finer (coarser) particle size distributions, thereby converging on similar DOD values despite fundamentally different representations of dust abundance. This compensation mechanism has been noted in previous intercomparison studies (Kim et al., 2019; Gliß et al., 2021) and highlights a limitation of using observation-estimated DOD alone as a constraint for model evaluation.

3.3 Dust vertical distributions

Beyond column-integrated quantities, the vertical distribution of dust governs its atmospheric lifetime and transport range, as particles at different altitudes experience varying wind patterns and removal processes. Dust vertical profiles in domain averages are obtained from 10 AeroCom P3 models with original vertical resolutions (Table 1), as shown in Figure 9, while the zonal mean dust vertical distribution is presented in Figure S6. The CALIOP dust extinction coefficients have upper and lower ranges derived from the upper and lower assumptions of dust and non-dust DPR at 532 nm (Yu et al., 2015a; Song et al., 2021), as described in Section S1.2.

The comparison reveals systematic regional variations in model performance against CALIOP. Over NAF, models generally capture near-surface dust concentration with extinction decreasing sharply with altitude, consistent with CALIOP peak values of 0.10-0.15 km^{-1} below 1 km, although GFDL-AM4, NorESM2, and ECHAM-SALSA show persistent underestimation within 5 km. Over GOG, observed extinction decreases to 0.02-0.03 km^{-1} with models reproducing vertical structure but showing substantial spread. EAO shows intermediate behavior with considerable inter-model diversity in both magnitude and vertical distribution. CAR exhibits the greatest model-observation discrepancy, with CALIOP indicating dust layers mainly within the marine boundary layer (1-3 km, 0.01-0.02 km^{-1}), yet models concentrate extinction at ~2 km (< 0.015 km^{-1}). However, it should be noted that CALIOP's dust retrieval relies on particulate depolarization ratio assumptions (δd = 0.2-0.3 for dust, δnd = 0.02-0.07 for non-dust), which may introduce high bias in marine boundary layers where nonspherical sea salt under low humidity can exhibit elevated depolarization (Ferrare et al., 2023). Large inter-model diversity across all regions indicates fundamental differences in model treatment of transport and deposition processes.

https://doi.org/10.5194/egusphere-2026-4322
Preprint. Discussion started: 17 August 2026

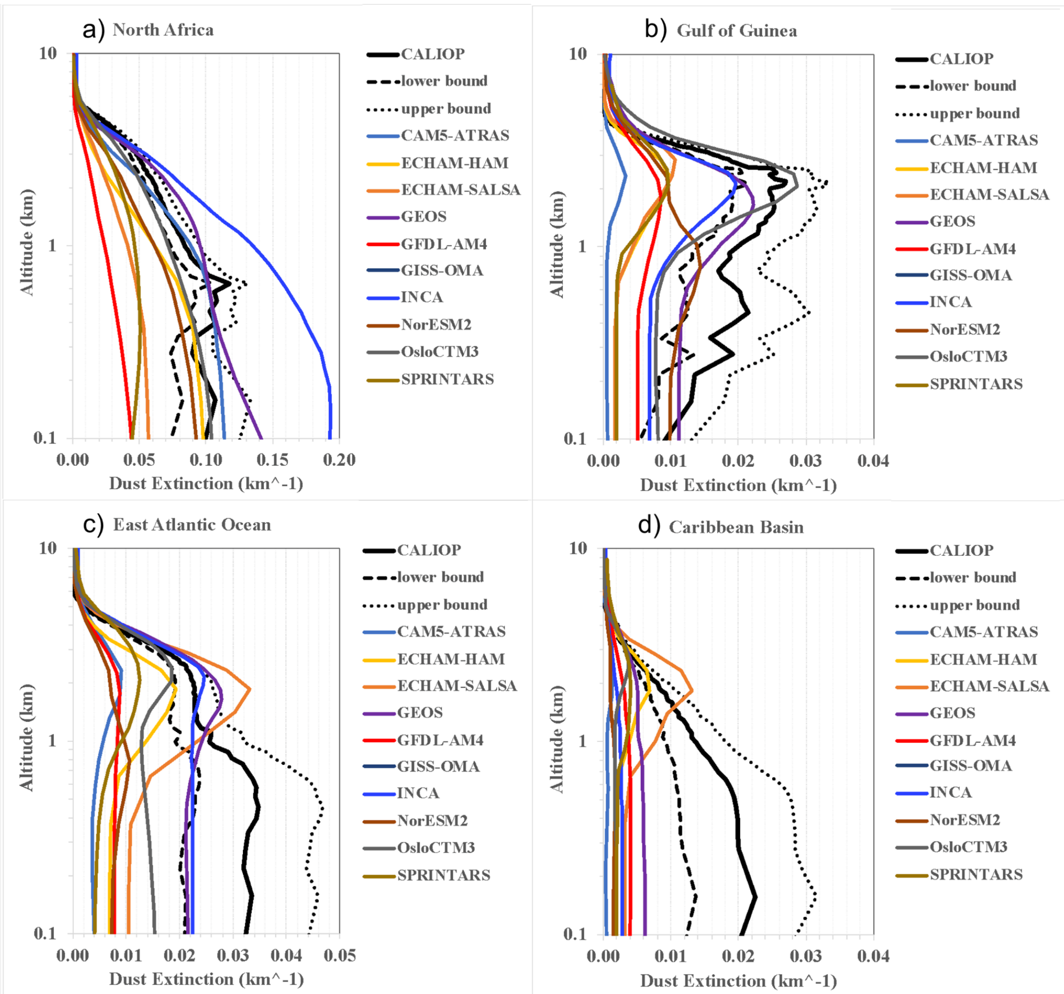

Figure 9: Annual mean vertical distribution of dust extinction coefficient (km⁻¹) at 532 nm in 2010 across the four transatlantic subregions: (a) North Africa, (b) Gulf of Guinea, (c) Eastern Atlantic Ocean, and (d) Caribbean Basin. The solid black line represents the CALIOP-derived extinction profile, with dashed and dotted lines denoting the lower and upper bounds of the observational uncertainty range. Colored lines correspond to individual model simulations.

3.4 Dust surface mass concentration

While the preceding sections constrain total atmospheric dust burden through column-integrated diagnostics, surface dust concentration provides a complementary perspective on boundary layer dust distribution, where dust directly affects air quality and human health (Zuidema et al., 2019; Prospero et al., 2014). This quantity is particularly sensitive to the vertical distribution evaluated in Section 3.3. In this section, we evaluate monthly surface concentrations in 2010 against ground-based measurements in Barbados (13°6′N, 59°37′W) and Miami (25°45′N, 80°15′W), as shown in Figure 10. Detailed spatial distribution from each available P3 model is shown in Figure S7. Note that the results of Group 3 models included in Figure 10 are analyzed separately in Section 3.7.

https://doi.org/10.5194/egusphere-2026-4322
Preprint. Discussion started: 17 August 2026

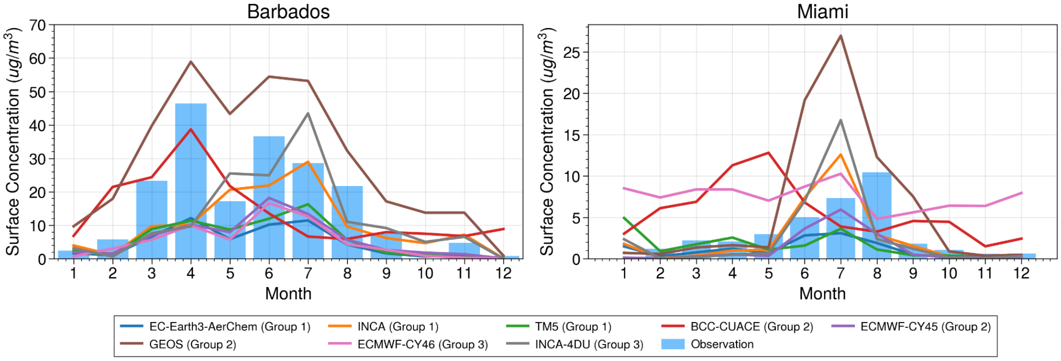

Figure 10: Monthly mean dust surface mass concentration (μg m⁻³) at (a) Barbados (13°6′N, 59°37′W) and (b) Miami (25°45′N, 80°15′W) for the year 2010. Blue bars represent observational measurements, while colored lines correspond to individual model simulations categorized into Group 1 (EC-Earth3-AerChem, INCA, TM5), Group 2 (GEOS, BCC-CUACE, ECMWF-CY45), and Group 3 (ECMWF-CY46, INCA-4DU).

At Ragged Point, Barbados, observations show pronounced seasonal cycles peaking in boreal spring-summer (March-August) when the ITCZ shifts northward and the Saharan Air Layer intensifies, reaching ~46 μg m^{-3} (April) and ~37 μg m^{-3} (June) before declining to <10 μg m^{-3} in fall-winter. GEOS produces the highest concentrations with well-aligned seasonality but overestimates by 30-50% over the year. BCC-CUACE captures the April maximum (~40 μg m^{-3}) but declines too rapidly. The three Group 1 models underestimate near-surface dust concentration by factors of 2-5 in spring and by 30-50% in summer. In Miami, observations show a concentrated summer maximum (~10 μg m^{-3} in August) with a wider inter-model spread than in Barbados. GEOS and INCA overestimate the summer peak by factors of 2-3, while BCC-CUACE overestimates in spring. Meanwhile, the two Group 1 models (EC-Earth3-AerChem and TM5) and ECMWF-CY45 remain at or below observations throughout the year.

Comparing the model performance between two regions, we found several models underestimate the summertime peak of near-surface concentrations at Barbados (60°W) yet overestimate those at Miami (80°W), possibly due to the uncertainty in simulating the ITCZ migrations and the challenges in reproducing the observed Central American dust barrier (80°W-90°W in CAR; Nowottnick et al., 2011) that could mitigate dust near-surface concentrations in Miami. In addition, None of the six models simultaneously reproduces seasonal cycles and magnitudes at both stations, underscoring the challenges in simulating the complete transatlantic dust pathway to receptor sites.

3.5 Dust deposition and loss frequency

The underestimation in DOD and mass loading documented in Section 3.2, together with the vertical profile biases in Section 3.3, should manifest as biases in dust deposition flux. Satellite-based dust deposition estimation in 2010 from Yu et al. (2019) provides a direct assessment of how these cumulative transport errors translate into surface fluxes over the open ocean. We also use a climatology of in-situ measurements of surface deposition fluxes from 42 sites for evaluations (see Section S2.1), which serve as an independent cross-check on the deposition estimates across the transatlantic corridor and over dust source regions (where satellite-based estimates are not available due to the presence of huge amounts of dust emissions).

https://doi.org/10.5194/egusphere-2026-4322
Preprint. Discussion started: 17 August 2026

In Figure 11, DustCOMM products and model median show peak deposition over NAF with a westward decrease across the Atlantic. DustCOMM-PM20 exhibits substantially higher deposition (200-2000 mg m⁻² day⁻¹) than PM10 (50-500 mg m⁻² day⁻¹) and model median (50-200 mg m⁻² day⁻¹), particularly over NAF and coastal EAO, due to the rapid settling of 10-20 μm particles. The model median captures spatial patterns but underestimates magnitudes over NAF compared to in-situ measurements, and EAO and CAR compared to satellite estimations. In-situ measurements span from <10 mg m⁻² day⁻¹ at remote sites to >500 mg m⁻² day⁻¹ near the African coast.

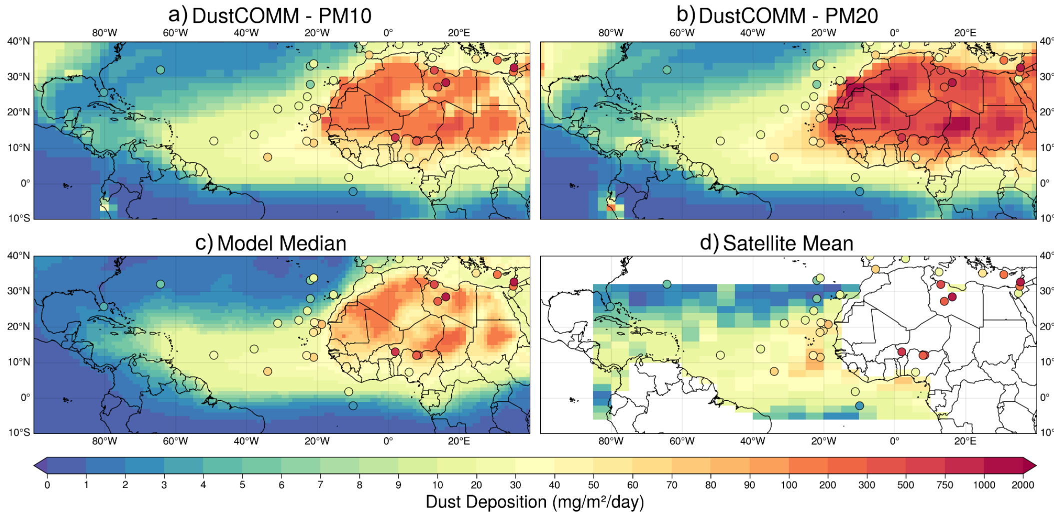

Figure 11: Annual mean dust deposition flux (mg m⁻² day⁻¹) across the transatlantic domain for the year 2010, as estimated by (a) DustCOMM-PM10, (b) DustCOMM-PM20, (c) the multi-model median, and (d) the satellite-derived mean. Colored circles denote 42 in-situ deposition measurements at surface stations, plotted on the same color scale for direct comparison.

Table 5 lists the main statistics from the comparisons of AeroCom P3 models and satellite estimates with the 42 in-situ measurements. Satellite estimates achieve the lowest RMSE over the ocean (26 sites) with a slight negative bias. DustCOMM-PM20 shows ~50% lower bias than DustCOMM-PM10 sharing similar correlations (42 sites). AeroCom P3 correlations range from 0.42-0.67, with Groups 2 exceeding Group 1, indicating improved transport representation with coarser particles. However, all products show systematic negative bias; most models underestimate by 54-101 mg m⁻² day⁻¹ regardless of size range, indicating excessive removal rates, although it should be noted that some in-situ measurements happened in the 1980s and early 1990s when African dust was more active.

Table 5: Correlations, mean bias, and RMSE for dust deposition from the satellite estimates, 2 DustCOMM products, and 15 models compared with the dust deposition climatology from the 42 in-situ measurements within the transatlantic region. The annual mean satellite-averaged dust deposition is compared with 26 sites over the tropical Atlantic Ocean.

Category	Source	Correlations	Mean Bias (mg m⁻² day⁻¹)	RMSE
Satellite-based estimate (ocean-	Mean of CALIOP, MODIS, MISR, and	0.689	-3.306	19.471

https://doi.org/10.5194/egusphere-2026-4322
Preprint. Discussion started: 17 August 2026

only)	IASI			
PSD-constrained model climatology	DustCOMM - PM10	0.687	-77.437	186.914
	DustCOMM - PM20	0.671	-27.046	145.755
AP3 Group 1 models	CAM5-ATRAS	0.608	-61.542	170.525
	EC-Earth3-AerChem	0.440	-96.891	206.758
	ECHAM-HAM	0.424	-85.298	200.449
	ECHAM-SALSA	0.208	-95.481	208.674
	INCA	0.547	-77.949	192.878
	NorESM2	0.532	-101.13	208.014
	TM5	0.359	-93.103	204.702
AP3 Group 2 models	BCC-CUACE	0.579	-54.604	165.936
	ECMWF-CY45	0.519	-78.018	183.794
	GEOS	0.583	-78.163	190.108
	GFDL-AM4	0.608	-87.808	196.335
	GISS-MATRIX	0.508	-93.998	201.966
	GISS-OMA	0.591	-80.512	186.847
	OsloCTM3	0.633	-74.021	182.601
	SPRINTARS	0.560	-80.309	183.355

To isolate uncertainty associated with dust removal processes from that resulting from dust emissions, we examine the loss frequency (deposition/loading ratio) representing the dust removal efficiency (Yu et al., 2019), as shown in Figure 12. Over NAF, model median is 0.18 day^{-1} with order-of-magnitude spread (~0.06-0.1 day^{-1} for ECHAM-SALSA/ECHAM-HAM/ INCA/GISS-MATRIX to about 0.6 day^{-1} or higher for SPRINTARS and BCC-CUACE), reflecting fundamental differences in gravitational settling and dry deposition parameterizations (the wet deposition over NAF is minimal). For DustCOMM, the loss frequency is more than a factor of two larger for PM20 than for PM10, which is consistent with the fact that the gravitational settling velocity is much higher for coarse particles than for fine particles. However, the model diversity in the loss frequency shows no consistent relationship with the cut-off size assumed among the models. Although all models calculate the gravitational settling velocity based on the same physical principles for spherical particles, the large model diversity in the dust loss frequency suggests that these models may differ substantially in dust size distributions and details in the parameterizations.

Over EAO and CAR, model median increases from 0.168 day^{-1} (EAO) to 0.296 day^{-1} (CAR), systematically exceeding satellite-estimated values by factors of 2-3. This confirms findings by Yu et al. (2019) and Wu et al. (2020) that models remain overestimating removal efficiency over the Atlantic, contributing to the documented underestimation of dust loading in remote downwind regions (Kim et al., 2014; Kok et al., 2021; Section 3.2). Over GOG, model median is comparable with satellite estimates (0.13-0.15 day^{-1}). Detailed spatial distribution of deposition and loss frequency from each model is shown in Figures S8 and S9.

https://doi.org/10.5194/egusphere-2026-4322
Preprint. Discussion started: 17 August 2026

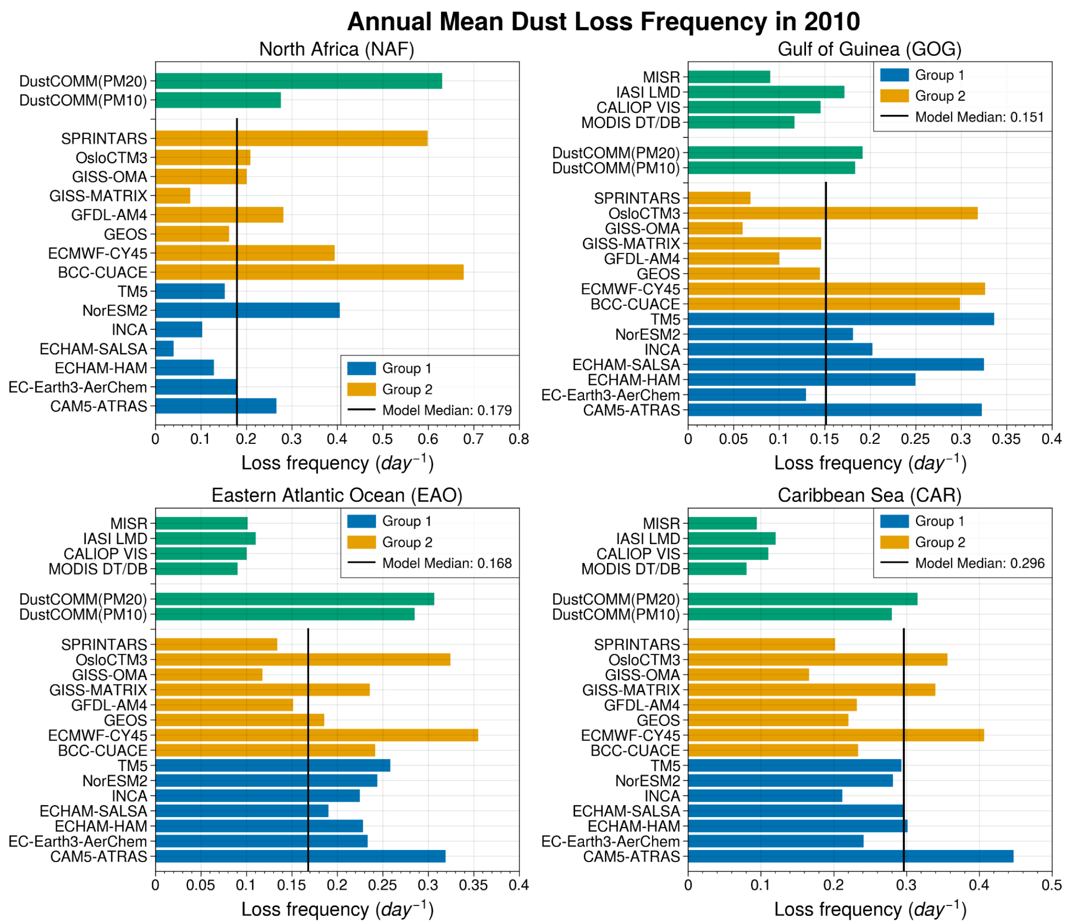

Figure 12: Annual mean dust loss frequency (day⁻¹) in 2010 across the four transatlantic subregions: (a) North Africa (NAF), (b) Gulf of Guinea (GOG), (c) Eastern Atlantic Ocean (EAO), and (d) Caribbean Sea (CAR). Green bars represent satellite-derived loss frequencies (from MODIS DT/DB, CALIOP, IASI, and MISR), and DustCOMM constrained estimates (PM10 and PM20). Blue and orange bars correspond to Group 1 and Group 2 model simulations, respectively. The vertical black line indicates the multi-model median for each subregion.

3.6 Surface precipitation rate

The overestimated loss frequencies documented in Section 3.5 could, in principle, arise partly from biases in wet scavenging determined by the combination of precipitation amount and the wet removal parameterizations. In this section, we evaluate the fidelity of precipitation fields from 12 P3 models by comparing with the GPCP observations as shown in Figure 13, to assess whether precipitation biases may contribute to the excessive dust loss.

Model medians generally agree with GPCP, with differences within 15%. Specifically, over NAF, BCC-CUACE and ECHAM-SALSA underestimate the precipitation rates by ~0.25 mm day^{-1}, though this moderately affects dust budgets since dry deposition dominates near sources. Over GOG, several models (GFDL-AM4, GEOS, BCC-CUACE, TM5) overestimate rainfall near the ITCZ (3.0-4.0 mm day^{-1}; see spatial distributions of specific models in Figure S10), enhancing

https://doi.org/10.5194/egusphere-2026-4322
Preprint. Discussion started: 17 August 2026

wet scavenging of southward-transported dust and contributing to elevated loss frequencies as mentioned in Section 3.5. Over EAO, the model median (2.9 mm day^{-1}) agrees well with GPCP within a few percent, although the models differ by a factor of 2 between the highest and lowest precipitation rates.

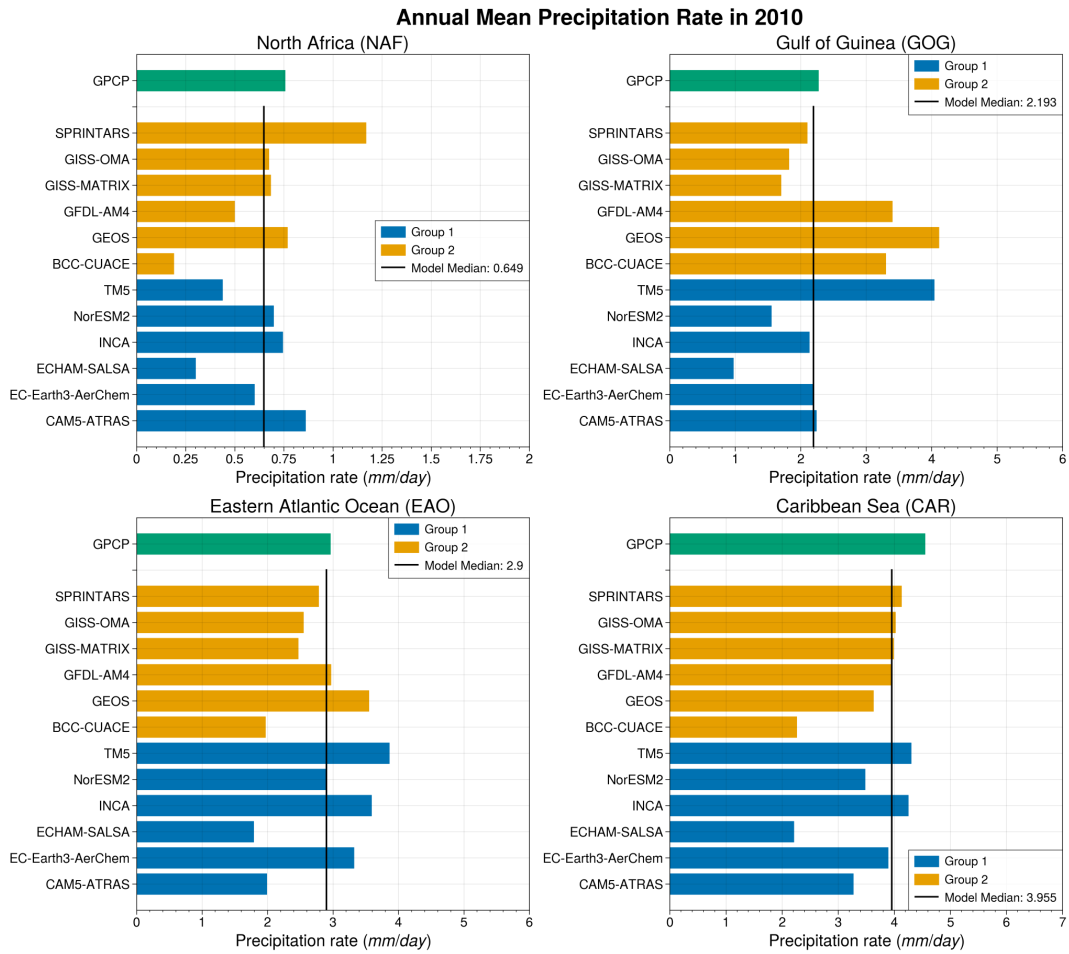

Figure 13: Annual mean precipitation rate (mm d) in 2010 across the four transatlantic subregions: (a) North Africa (NAF), (b) Gulf of Guinea (GOG), (c) Eastern Atlantic Ocean (EAO), and (d) Caribbean Sea (CAR). Green bars represent the Global Precipitation Climatology Project (GPCP) observational estimate, while blue and orange bars correspond to Group 1 and Group 2 model simulations, respectively. The vertical black line denotes the multi-model median for each subregion.

Over CAR, the model median (3.9 mm day^{-1}) underestimates GPCP (4.6 mm day^{-1}) by ~15%. This reduced precipitation rate indicates reduced wet scavenging that favors dust retention, yet models still substantially underestimate DOD and mass loading in CAR (Section 3.2). The results reinforce the findings in Sections 3.3 and 3.4 that excessive gravitational settling, rather than wet removal, is likely to serve as the main driver of premature dust loss during transatlantic transport (Meng et al., 2022).

https://doi.org/10.5194/egusphere-2026-4322
Preprint. Discussion started: 17 August 2026

3.7 Evolution of model representations of super-coarse dust

The preceding sections found a systematic underestimation of dust mass loading, deposition, and DOD that deteriorates with transport distance (Sections 3.2–3.4), coupled with an overestimation of loss frequency (Section 3.4), collectively pointing to an inadequate representation of coarse and super-coarse particles in the AeroCom P3 ensemble. The enhanced super-coarse dust representations in ECMWF (ECMWF-CY46) and INCA (INCA-4DU) models provide an opportunity to assess whether these configurations improve transatlantic dust simulation when compared with their predecessors. Therefore, in this section, we first evaluate both versions of the two models against AERONET DOD and derived mass loading, and in-situ deposition climatology, as presented in Table 6.

Table 6: Main statistics of comparisons of DOD, mass loading, depositions from the series of ECMWF and INCA models with those from 19 AERONET sites and 42 in-situ measurements, respectively. Mean bias is used for DOD and deposition comparison, while relative difference is used for mass loading comparison.

Category	Model	Correlations	Mean Bias or Relative Difference (%)	RMSE
DOD compared with 19 AERONET sites	ECMWF-CY45	0.938	-24.98%	0.059
	ECMWF-CY46	0.941	-13.5%	0.050
	INCA	0.923	37.14%	0.095
	INCA-4DU	0.906	33.08%	0.093
Mass loading (g m^{-2}) compared with 19 AERONET sites	ECMWF-CY45	0.833	-83.07%	0.888
	ECMWF-CY46	0.886	-64.36%	0.691
	INCA	0.874	-67.95%	0.753
	INCA-4DU	0.837	-32.44%	0.486
Deposition (mg m^{-2} d^{-1}) compared with 42 in-situ measurements	ECMWF-CY45	0.519	-78.018	183.794
	ECMWF-CY46	0.674	-5.179	145.337
	INCA	0.547	-77.949	192.878
	INCA-4DU	0.554	228.955	600.552

Similar to other P3 models, all four models DOD show high correlations (> 0.9), moderate biases (-25% to 37%), and low RMSE (0.05 to 0.10) against AERONET coarse AOD. For the comparison of dust mass loading, Group 3 models (ECMWF-CY46 and INCA-4DU) reduce the bias by up to ~50%, with INCA-4DU achieving the smallest relative difference (−32%) and RMSE (0.48), reflecting the benefit of including super-coarse particles in models. For comparison with in-situ dust deposition climatology, INCA-4DU overestimates by a factor > 3 with an RMSE 3 to 4 times larger than the P3 ensemble, likely from extended size distribution and the corresponding excessive mass loadings from super-coarse particles, while with aggressive removal. ECMWF-CY46 achieves the lowest RMSE (~15-20% below the P3 ensemble shown in Table 5) with bias reduced by ~20% from ECMWF-CY45, and correlation (0.67) comparable to satellite estimates (0.68 in Table 5).

Additionally, we compare the four models against DustCOMM and satellite observations across transport regions (GOG+EAO+CAR) as well as NAF emissions, as shown in Figure 14. Detailed spatial distribution of all dust characteristics for the two pairs of models is presented in Figures S11 and S12.

https://doi.org/10.5194/egusphere-2026-4322
Preprint. Discussion started: 17 August 2026

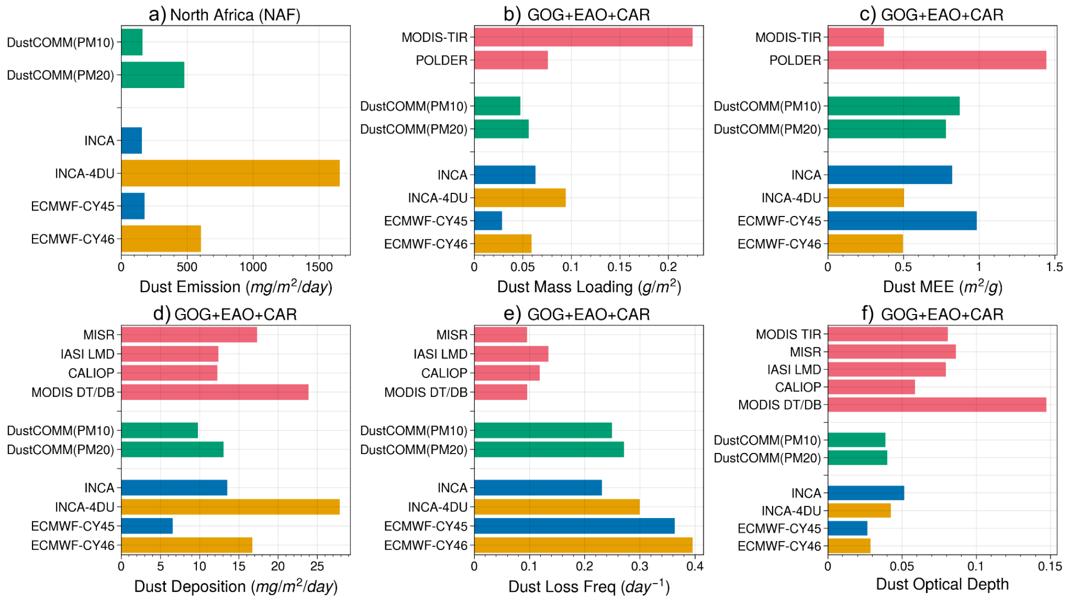

Figure 14: Summary comparison of key dust cycle variables for selected models (INCA, INCA-4DU, ECMWF-CY45, ECMWF-CY46) and DustCOMM products over NAF (a) and downwind transport regions combined (GOG + EAO + CAR, the rest of the panels). Variables include (a) dust emission flux (mg m^{-2} day^{-1}), (b) dust mass loading (g m^{-2}), (c) dust MEE at 550 nm (m^2 g^{-1}), (d) dust deposition flux (mg m^{-2} day^{-1}), (e) dust loss frequency (day^{-1}), and (f) dust optical depth. Pink bars denote satellite-derived estimates. Green bars represent DustCOMM constrained estimates (PM10 and PM20). Blue bars correspond to INCA and ECMWF-CY45; orange bars correspond to INCA-4DU and ECMWF-CY46.

Over NAF, INCA-4DU's emission flux exceeds ~1600 mg m^{-2} day^{-1}, ~10 times the INCA value, driven by the additional two coarse and one fine dust modes that significantly expand the size range from INCA. However, INCA-4DU's 10-fold emission increase yields only ~30% more transport-region mass loading compared to INCA, as super-coarse particles settle gravitationally before reaching long-range transport regions (see INCA models inter-comparisons in Figure S12). ECMWF-CY46 triples emissions from ~200 to ~600 mg m^{-2} day^{-1} through mass reallocation to super-coarse bins (98.45% vs 84%) and updated source maps (see spatial emissions in Figure S11). Comparably, ECMWF-CY46 nearly doubles transport-region loading (0.075 vs 0.04 g m^{-2}), closer to that of DustCOMM PM20. In the meantime, because the super-coarse dust is optically insensitive at visible wavelengths, as mentioned in Section 3.2, with greater contributions from coarse particles in size distributions, the effective MEE of INCA-4DU and ECMWF-CY46 drops 37% (~0.8 from INCA to ~0.5 m^2 g^{-1}), and 50% (~1.0 m^2 g^{-1} from CY45 to ~0.5 m^2 g^{-1}), respectively. Consequently, the reduced MEEs lead to insignificant changes of mid-visible DOD compared to their predecessors, remaining underestimated relative to satellite DODs.

Reflected by the increased emissions and mass, deposition in transport regions from INCA-4DU increases ~50% versus INCA (27.5 mg m^{-2} day^{-1}), exceeding in-situ measurements (Table 6), DustCOMM PM20 (~13 mg m^{-2} day^{-1}) and all satellite estimates (13-24 mg m^{-2} day^{-1}) by a factor of 2-3. ECMWF-CY46 increases deposition to ~17 versus ~7 mg m^{-2} day^{-1} for CY45, falling within satellite range with the lowest RMSE/bias against in-situ measurements among P3 models

https://doi.org/10.5194/egusphere-2026-4322
Preprint. Discussion started: 17 August 2026

(Table 6), though correlations decrease ~20% due to long-range transport mismatches (see ECMWF models inter-comparisons in Figure S13). However, loss frequencies of both models exceed satellite estimates (0.1–0.12 day^{-1}), reinforcing that models systematically overestimate removal efficiency even when deposition magnitudes improve (e.g., ECMWF-CY46), likely compensated by higher emissions .

For surface mass concentration presented in Figure 10 of Section 3.4, at Ragged Point, Barbados, we found that INCA/INCA-4DU and ECMWF-CY45/CY46 produce similar seasonal variations, while both pairs of models miss the maximum in spring. ECMWF-CY45/CY46 have low concentrations (<20 μg m^{-3}) year-round, underestimating near-surface dust concentrations despite the much broader size ranges (up to 40 μm, see Table 1). However, at Miami, while ECMWF-CY45 captures the summer peak, ECMWF-CY46 overestimates the near-surface concentrations by factors of 2-3 throughout the year, possibly due to the increasing emission of dust sources in North America (Figure S13). INCA and INCA-4DU both overestimate the summer peak by factors of 2-3, indicating limited improvements of increasing contributions of super-coarse particles for surface concentrations in long-range transport regions.

4. Discussions

4.1 DOD diversity in AeroCom P3 models

Diversity in mid-visible DOD among AeroCom P3 models is relatively low (30–45%). Specifically, the diversity in DOD over NAF largely reflects differences in dust source maps and emission parameterizations (Figure 2 and Figure S1), where models disagree on the spatial extent and intensity of active dust sources across the Sahara and Sahel. Over the transport regions, the DOD discrepancy with satellite observations progressively increases with distance from the source, with multi-model median DOD ~50% lower than satellite estimates over EAO and GOG and ~70% lower over CAR (Figure 5). This systematic underestimation is consistent across nearly all models regardless of their emission magnitudes, indicating that the source of bias propagates from emission in NAF to the removal process during transport.

In addition, the relatively low diversity in mid-visible DOD among AeroCom P3 models may not be interpreted as evidence that simulations of dust cycles have converged toward the observational estimate. Firstly, the inter-model spread remains significant in vertical dust extinction profiles (Figure 9) despite the relatively low DOD diversity, which could amplify the biases in depositions and surface concentrations that originate at emission (Koffi et al., 2016; Koffi et al., 2012). Secondly, as documented in Section 3.2, the apparent agreement in DOD masks compensatory biases between mass loading and MEE, where models with low (high) dust mass are compensated by a high (low) MEE to produce similar DOD values. This compensation also limits what assimilation can deliver. MERRA-2 and CAMS assimilate satellite total AODs (Buchard et al., 2017; Randles et al., 2017; Inness et al., 2019), which improve the DOD characterization (Table 3), while carrying mass loadings well below the MODIS-TIR and AERONET-GRASP estimates (Figures 4 and 6), as the column mass, vertical distribution, and deposition depend heavily on each system's own size distribution, MEE, and transport. Thus, even though an AOD-constrained reanalysis can reproduce the observed AOD, it retains mass fields inconsistent with observation-based estimates due to the same compensation identified among models.

The introduction of emerging thermal infrared DOD and polarimetric aerosol component products

https://doi.org/10.5194/egusphere-2026-4322
Preprint. Discussion started: 17 August 2026

(i.e., MODIS-TIR, IASI and POLDER retrievals) provides size-aware and component-specific observational constraints that reveal biases not apparent in standard mid-visible DOD comparisons, particularly for the coarse-mode portion that dominates the dust mass budget. However, in this study, the thermal infrared DOD is converted to mid-visible DOD because DOD at 10 μm is not reported by the models in the AeroCom P3 CTRL experiment. In addition, it is challenging to estimate the contributions of coarse-mode dust as the size distribution is handled vastly differently among the models. A specific AeroCom model experiment involving a smaller number of models has been designed to jointly assess DOD and MEE in both mid-visible and thermal infrared as well as associated dust mass budget, and the results are currently being synthesized (D. Kim et al., 2026, manuscript in preparation). Therefore, DOD at 10 μm is strongly suggested to be included in future AeroCom experiments, as it reflects the impacts of dust microphysical and optical properties from models. To better evaluate the size-aware dust properties, including size-segregated outputs from models, for example, with diameter less than 1 μm (PM1.0), 2.5 μm (PM2.5), 10 μm (PM10), and 20 μm (PM20), is highly recommended.

4.2 Dust microphysical properties as the central driver of model biases

As discussed in Section 3, inter-model and model–observation discrepancies often follow systematic patterns rooted primarily in the representation of dust particle size distribution and, to a lesser extent, particle shape. While differences in emission sources and schemes among AeroCom P3 models set the stage, it is the assumed microphysical properties (e.g., size distributions, particle shapes) that propagate through the entire dust cycle from optical properties to vertical transport and further to removal efficiency.

First of all, the truncation of the size distribution in most models matters little for mid-visible DOD, because coarse particles (e.g., D > 15 μm) contribute substantial mass but little extinction at 550 nm (Zheng et al., 2024). Therefore, increasing contributions of super-coarse dust, including upper size limit extension, would change mass loading and MEE in opposite directions and lead to nearly unchanged DOD, as demonstrated by DustCOMM PM10 and PM20 comparisons (Figures 5-8) and Group 3 model comparisons with their predecessors (Figure 14). Specifically, we found Group 3 models (INCA-4DU and ECMWF-CY46) indeed increase mass loading by 30%-50% over transport regions compared with their predecessors (INCA and ECMWF-CY45), although it may still not be enough with respect to observation-based estimations (e.g., AERONET and MODIS-TIR) due to the persistently overestimated loss frequencies. However, their effective MEE decreased by 30%-50%, leading to limited improvements in DOD simulations. In addition, there are insignificant differences of mid-visible DOD among the three groups of models with variation upper limits of size distributions, while most of P3 models still underestimate DOD relative to satellite over transport regions (GOG+EAO+CAR) (Figures 4-5), even though some models overestimated DOD over NAF (with positive biases listed in Table 3).

Secondly, models' MEE relative to in-situ and satellite estimates (Section 3.2) are found to be systematically overestimated, implying that the model-simulated size distributions are possibly biased toward fine particles. Here, in-situ measurements and most models applied the spherical-shape assumption (except GEOS with a spheroid assumption), which has only a secondary effect on MEE in the mid-visible (Mishchenko et al., 1995; Hansell et al., 2011; Colarco et al., 2014). Consequently, if models expand the emitted particle size upper limits with greater contributions of coarse particles in size distributions, their emission flux, mass loading would increase with

https://doi.org/10.5194/egusphere-2026-4322
Preprint. Discussion started: 17 August 2026

decreasing MEE correspondingly.

However, as demonstrated by the Group 3 models in Section 3.7, INCA-4DU's four-mode configuration dramatically increases emissions and deposition, yet fails to improve DOD or mass loading over transport regions because 20–40 μm particles have limited sensitivity in mid-visible and are removed too rapidly. ECMWF-CY46's mass reallocation shifts deposition and mass loading closer to observational estimates, but with loss frequency remaining excessively overestimated. Neither of the two models resolves the persistent DOD underestimation and excessive loss frequency downwind. The precipitation analysis (Section 3.6) confirms that model median precipitation rates are broadly consistent with GPCP observations, implicating the parameterization of size-dependent removals, rather than precipitation rate biases, as the primary driver for over-efficient dust removal. As a result, broadening the size range with a coarser size distribution, although necessary, is still insufficient.

There are two possible missing ingredients. One is the potential additional mechanisms that could reduce the gravity settling velocity for super-coarse to giant dust particles, such as electromagnetic forces (Renard et al., 2018; Toth III et al., 2020), turbulent mixing (Cornwell et al., 2021; Rodakoviski et al., 2023), and convective uplift (Gasteiger et al., 2017). The other is the concurrent incorporation of dust non-sphericity in gravitational settling, which would reduce settling velocities by 10-30% (Huang et al., 2020; Ginoux, 2003), extending atmospheric residence times and increasing the dust mass loading.

However, it is important to note that independent mass loading estimates from POLDER, the MODIS-TIR, and AERONET-based products also show diverse results: P3 models agree more with POLDER while being significantly lower than those from MODIS-TIR and AERONET estimates. With such large spreads in mass loading estimations from observations, we strongly suggest further improvements in remote sensing retrievals of dust properties, including not only DOD but also particle size distributions, mass loadings, and vertical distributions.

Beyond the size and shape assumptions emphasized above, broader uncertainties in dust optical properties further complicate model–satellite intercomparisons, which should be acknowledged in this study. As highlighted by Castellanos et al. (2024), the dust optical properties assumed or retrieved by remote sensing algorithms and global circulation models are often not internally consistent within individual models or retrievals, and they diverge between models and retrievals, for example, the diversity of DOD (Figure 4) and mass loading (Figure 6). To rigorously diagnose model performance, the implementation of observation simulators is also recommended, together with forward modeling in the context of observing system simulation experiments (OSSEs; Castellanos et al., 2018), which could elucidate these biases and quantify their sensitivities to model and retrieval assumptions.

5. Conclusions

This study evaluates transatlantic dust simulations from 17 AeroCom P3 models against a multi-platform observational framework spanning dust emissions, DOD, mass loading, MEE, vertical profiles, deposition, loss frequency, surface concentration, and precipitation across the Saharan dust transport pathway. The end-to-end, multi-variable assessment yields several insights for guiding future model development and observational strategy.

https://doi.org/10.5194/egusphere-2026-4322
Preprint. Discussion started: 17 August 2026

First, mid-visible DOD alone is an insufficient metric for evaluating dust model performance because of its dependence on particle size distribution and weak sensitivity to coarse and super-coarse particles. Although AeroCom P3 models slightly reduced DOD diversity to 30–45% across the transport domain compared to AeroCom P2 (38–59%; Kim et al., 2014), biases between dust mass loading and MEE remain. Future benchmarking should therefore require joint reporting of DOD at 550 nm and 10 µm complemented by size-segregated outputs (e.g., PM1.0, PM2.5, PM10, PM20), as a diagnostic triplet, to evaluate the size-dependent removal processes.

Second, the dominant ensemble-wide bias is a distance-dependent underestimation of dust burden that intensifies along the transport pathway. The two updated models (INCA-4DU and ECMWF-CY46) show examples that broadening the size range with increased coarse-mode contributions do not resolve the persistent DOD and mass loading underestimation and overestimated loss frequency over downwind regions. The persistent bias is thus more likely due to a combination of parameterization deficiencies of size-dependent gravitational settling, vertical transport, wet scavenging, and the inadequate representation of free-tropospheric turbulence processes.

Impacts of such biases are also beyond model diagnostics. Dust over the tropical Atlantic cools the surface and suppresses hurricane activity through direct and semi-direct radiative effects (Evan et al., 2006; Zhang et al., 2007; Di Biagio et al., 2020); an ensemble low by 50–70% in downwind burden will understate this influence, and coarse and super-coarse particles carry disproportionate weight in the longwave (Kok et al., 2017; Adebiyi and Kok, 2020). The same deficit in coarse dust mass propagates to the number and surface area available for ice nucleation (Karydis et al., 2011) and to the iron and phosphorus flux that fertilizes the tropical Atlantic and the Amazon basin (Yu et al., 2015b; Westberry et al., 2022), with attendant consequences for carbon cycle estimates (Maher et al., 2010). Because the bias increases monotonically with transport distance rather than varying randomly among models, it acts as a structural error in ensemble-based assessments of dust radiative forcing and dust-mediated biogeochemistry, and cannot be reduced by averaging across models. Therefore, the priorities for the modeling community are suggested to represent emitted size distributions with sufficient fine- and coarse- particle mass with extended upper size limits, adopt non-spherical optics, and explore additional physical mechanisms that reduce the overestimated removal efficiency in both fine and coarse mode.

Third, the MODIS-TIR and POLDER retrievals in this study introduced comparisons of dust mass loadings with AeroCom models, yet the approximation of retrieved quantities (e.g., coarse-mode components and insoluble components) that are not directly dust yields inconsistency in the comparison. Expanding the use of thermal-infrared and polarimetric satellite retrievals sensitive to coarse dust microphysics, together with targeted field campaigns measuring size-resolved dust fluxes during long-range transport, will be essential for constraining these process-level uncertainties.

Finally, dust deposition is an important quantity that links the dust cycle with the carbon cycle, which has important implications for biogeochemical cycles and climate change. In-situ dust deposition measurements or proxies are scarce and only the climatology of annual dust deposition over limited regions is available to assess the models' performance in general. However, dust deposition varies substantially on a daily and seasonal basis. Although the satellite-based estimates

https://doi.org/10.5194/egusphere-2026-4322
Preprint. Discussion started: 17 August 2026

of seasonal mean dust deposition into oceans with the flux-divergency approach fill important spatial and temporal gaps, such estimates are subject to large uncertainties associated with satellite retrievals of dust optical depth and vertical distribution, as well as assumptions of dust MEE. Future satellite missions should improve dust quantification with enhanced technologies to better distinguish dust particles from other types of aerosol.

Appendix A: Glossary of Acronyms

AERONET: Aerosol Robotic Network
AOD: Aerosol Optical Depth
BCC-CUACE: Beijing Climate Center – China University of Aerosol Composition and Environment
BCC-GCM: Beijing Climate Center General Circulation Model
CALIOP: Cloud-Aerosol Lidar with Orthogonal Polarization
CALIPSO: Cloud-Aerosol Lidar and Infrared Pathfinder Satellite Observations
CAM5-ATRAS: Community Atmosphere Model version 5 – Aerosol Two-dimensional bin module for foRmation and Aging Simulation
CAMS: Copernicus Atmosphere Monitoring Service
CAR: Caribbean Sea
CCN: Cloud Condensation Nuclei
CNAI: Coarse-mode Non-Absorbing Insoluble (AERONET GRASP component)
CTRL: Control (AeroCom experiment configuration)
DB: Deep Blue (MODIS retrieval algorithm)
DEAD: Dust Entrainment and Deposition (emission scheme)
DOD: Dust Optical Depth
DT: Dark Target (MODIS retrieval algorithm)
DustCOMM: Dust Constraints from joint Observational-Modelling-experiMental analysis
EAO: Eastern Atlantic Ocean
EC-Earth3-AerChem: European Consortium Earth System Model version 3 configuration with interactive aerosols and atmospheric chemistry
ECHAM-HAM: European Centre Hamburg Atmospheric Model – Hamburg Aerosol Module
ECHAM-SALSA: European Centre Hamburg Atmospheric Model – Sectional Aerosol module for Large Scale Applications
ECMWF: European Centre for Medium-Range Weather Forecasts
ECMWF-CY45: ECMWF Integrated Forecasting System Cycle 45
ECMWF-CY46: ECMWF Integrated Forecasting System Cycle 46
ERA-Interim: ECMWF Re-Analysis Interim
FMF: Fine-Mode Fraction
FNAI: Fine-mode Non-Absorbing Insoluble (AERONET GRASP component)
GEOS: Goddard Earth Observing System
GFDL-AM4: Geophysical Fluid Dynamics Laboratory Atmospheric Model version 4
GISS-MATRIX: Goddard Institute for Space Studies – Multiconfiguration Aerosol TRacker of mIXing state
GISS-OMA: Goddard Institute for Space Studies – One-Moment Aerosol
GOCART: Goddard Chemistry Aerosol Radiation and Transport
GOG: Gulf of Guinea
GPCP: Global Precipitation Climatology Project

https://doi.org/10.5194/egusphere-2026-4322
Preprint. Discussion started: 17 August 2026

GRASP: Generalized Retrieval of Atmosphere and Surface Properties
IASI: Infrared Atmospheric Sounding Interferometer
IFS: Integrated Forecasting System (ECMWF)
INCA: INteraction with Chemistry and Aerosols
INCA-4DU: INCA with four dust modes
ITCZ: Intertropical Convergence Zone
LMD: Laboratoire de Météorologie Dynamique
MEE: Mass Extinction Efficiency
MERRA-2: Modern-Era Retrospective analysis for Research and Applications, Version 2
MISR: Multi-angle Imaging SpectroRadiometer
MMD: Mass Median Diameter
MODIS: Moderate Resolution Imaging Spectroradiometer
MODIS-TIR: MODIS Thermal Infrared (dust retrieval product)
NAF: North Africa
NorESM2: Norwegian Earth System Model version 2
OsloCTM3: Oslo Chemical Transport Model version 3
P1/P2/P3: AeroCom Phase I / Phase II / Phase III
PARASOL: Polarization and Anisotropy of Reflectances for Atmospheric Sciences coupled with Observations from a Lidar
PDR: Particulate Depolarization Ratio
PM10/PM20: Particulate Matter with diameter less than 10/20 µm (DustCOMM size cuts)
POLDER: Polarization and Directionality of the Earth's Reflectances
PSD: Particle Size Distribution
RMSE: Root Mean Square Error
SAL: Saharan Air Layer
SDA: Spectral Deconvolution Algorithm
SPRINTARS: Spectral Radiation-Transport Model for Aerosol Species
TIR: Thermal Infrared
TM5: Tracer Model version 5

Data availability:
The AeroCom Phase III model output is available through the AeroCom data server (https://aerocom.met.no/data; access requires authorization from the AeroCom team). MODIS Collection 6.1 aerosol products (Dark Target and Deep Blue) are available from NASA LAADS DAAC (https://ladsweb.modaps.eosdis.nasa.gov/). MISR Version 23 aerosol products are available from the NASA Atmospheric Science Data Center (https://asdc.larc.nasa.gov/project/MISR/). The CALIOP- and MODIS-derived global dust optical depth climatology from Song et al. (2021) is available at https://acros.umbc.edu/data-and-models/decadal-global-dust-aod-database/. The IASI-LMD dust optical depth product is available from the AERIS data center (https://iasi.aeris-data.fr/). The MODIS-TIR dust optical depth and effective diameter product is available in Zheng et al. (2026). The POLDER-3/GRASP component aerosol product (Li et al., 2022) is available from GRASP-Open (https://www.grasp-open.com/products/polder-data-release/). AERONET Level 2.0 SDA data are available from the AERONET data portal (https://aeronet.gsfc.nasa.gov/cgi-bin/webtool_aod_v3). The AERONET GRASP component retrieval product (Zhang et al., 2024) is available from GRASP-Open (https://www.grasp-open.com/products/). The DustCOMM version 1 dataset (Adebiyi et al., 2020;

https://doi.org/10.5194/egusphere-2026-4322
Preprint. Discussion started: 17 August 2026

Kok et al., 2021) is available from Zenodo (https://doi.org/10.5281/zenodo.2620475). The GPCP Version 2.3 monthly precipitation data (Adler et al., 2018) are available from NOAA NCEI (https://www.ncei.noaa.gov/data/global-precipitation-climatology-project-gpcp-monthly/). The Barbados and Miami surface dust mass concentration records (Zuidema et al., 2019) are available at https://doi.org/10.17604/q3vf-8m31. The sediment trap dust deposition data from the transatlantic region are available from PANGAEA: Friese et al. (2017) at https://doi.org/10.1594/PANGAEA.860539 and Korte et al. (2017) at https://doi.org/10.1594/PANGAEA.872089.

Author contributions:
JZ, HY and CR conceptualize the study; MC, MS, YB, SEB, HB, PC, DK, RCG, PG, ZK, HK, PLS, MTL, GM, HM, DJLO, SR, OS, and TT performed the AeroCom Phase III model experiments; JZ, HY, YD, OD, QS, JFK, LL, DW, ZZ developed the observational data; JZ, HY and CR collected and analyzed the data; JZ wrote the manuscript draft; all co-authors reviewed and edited the manuscript.

Competing interests:
At least one of the co-authors is a member of the editorial board of Atmospheric Chemistry and Physics.

Acknowledgement:
The study was supported by NASA Earth Sciences programs, including the Making Earth System Data Records for Use in Research Environments - MEaSUREs program managed by Dr. Lucia Tsaoussi (a project entitled “Development of a Comprehensive and Augmented Multi-Decadal Remote-Sensing Observations of Dust (CAMRO-Dust) Data Record for Earth Science Research and Applications”), the CALIPSO/CloudSat Science Team Recompete managed by Dr. David Considine, and the Cloud Credits Supplement to Enable Open Sciences for MEaSUREs and EMIT projects managed by Dr. Steven Crawford. The ECHAM-HAMMOZ model is developed by a consortium composed of ETH Zurich, Max Planck Institut für Meteorologie, Forschungszentrum Jülich, University of Oxford, the Finnish Meteorological Institute and the Leibniz Institute for Tropospheric Research, and managed by the Leibniz Institute for Tropospheric Research (TROPOS). H.M. was supported by the MEXT/JSPS KAKENHI Grant Numbers JP23K18519, JP23K24976, JP24H02225, JP26K00780, and JP26K03065; the MEXT Arctic Challenge for Sustainability II (ArCS II; JPMXD1420318865) and 3 (ArCS-3; JPMXD1720251001) projects; by the Environment Research and Technology Development Fund 2–2301 (JPMEERF20232001) and 2–2602 (JPMEERF20262002) of the Environmental Restoration and Conservation Agency; and by National Institute of Polar Research (NIPR) through Special Collaboration Project no. B25-02.

https://doi.org/10.5194/egusphere-2026-4322
Preprint. Discussion started: 17 August 2026

Reference:

Adebiyi, A., Kok, J. F., Murray, B. J., Ryder, C. L., Stuut, J.-B. W., Kahn, R. A., Knippertz, P., Formenti, P., Mahowald, N. M., Pérez García-Pando, C., Klose, M., Ansmann, A., Samset, B. H., Ito, A., Balkanski, Y., Di Biagio, C., Romanias, M. N., Huang, Y., and Meng, J.: A review of coarse mineral dust in the Earth system, Aeolian Res, 60, 100849, https://doi.org/10.1016/j.aeolia.2022.100849, 2023.

Adebiyi, A. A. and Kok, J. F.: Climate models miss most of the coarse dust in the atmosphere, Sci Adv, 6, eaaz9507, https://doi.org/10.1126/sciadv.aaz9507, 2020.

Adebiyi, A. A., Kok, J. F., Wang, Y., Ito, A., Ridley, D. A., Nabat, P., and Zhao, C.: Dust Constraints from joint Observational-Modelling-experiMental analysis (DustCOMM): comparison with measurements and model simulations, Atmos. Chem. Phys., 20, 829-863, https://doi.org/10.5194/acp-20-829-2020, 2020.

Adler, R. F., Sapiano, M. R. P., Huffman, G. J., Wang, J.-J., Gu, G., Bolvin, D., Chiu, L., Schneider, U., Becker, A., Nelkin, E., Xie, P., Ferraro, R., and Shin, D.-B.: The Global Precipitation Climatology Project (GPCP) Monthly Analysis (New Version 2.3) and a Review of 2017 Global Precipitation, Atmosphere, 9, 138, 2018.

Albani, S., Mahowald, N. M., Perry, A. T., Scanza, R. A., Zender, C. S., Heavens, N. G., Maggi, V., Kok, J. F., and Otto-Bliesner, B. L.: Improved dust representation in the Community Atmosphere Model, Journal of Advances in Modeling Earth Systems, 6, 541-570, https://doi.org/10.1002/2013MS000279, 2014.

Anderson, R. F., Cheng, H., Edwards, R. L., Fleisher, M. Q., Hayes, C. T., Huang, K.-F., Kadko, D., Lam, P. J., Landing, W. M., Lao, Y., Lu, Y., Measures, C. I., Moran, S. B., Morton, P. L., Ohnemus, D. C., Robinson, L. F., and Shelley, R. U.: How well can we quantify dust deposition to the ocean?, Philosophical Transactions of the Royal Society A: Mathematical, Physical and Engineering Sciences, 374, https://doi.org/10.1098/rsta.2015.0285, 2016.

Anderson, T. L., Wu, Y., Chu, D. A., Schmid, B., Redemann, J., and Dubovik, O.: Testing the MODIS satellite retrieval of aerosol fine-mode fraction, J Geophys Res Atmospheres, 110, https://doi.org/10.1029/2005JD005978, 2005.

Audoux, T., Laurent, B., Marticorena, B., Bergametti, G., Rajot, J. L., Féron, A., and Gaimoz, C.: Wet Deposition Fluxes of Mineral Dust and Their Relation With Cold Pools in the Central Sahel, Geophys Res Lett, 49, e2021GL095005, https://doi.org/10.1029/2021GL095005, 2022.

Bauer, S. E., Wright, D. L., Koch, D., Lewis, E. R., McGraw, R., Chang, L. S., Schwartz, S. E., and Ruedy, R.: MATRIX (Multiconfiguration Aerosol TRacker of mIXing state): an aerosol microphysical module for global atmospheric models, Atmos. Chem. Phys., 8, 6003-6035, https://doi.org/10.5194/acp-8-6003-2008, 2008.

Bauer, S. E., Tsigaridis, K., Faluvegi, G., Kelley, M., Lo, K. K., Miller, R. L., Nazarenko, L., Schmidt, G. A., and Wu, J.: Historical (1850–2014) Aerosol Evolution and Role on Climate Forcing Using the GISS ModelE2.1 Contribution to CMIP6, Journal of Advances in Modeling Earth Systems, 12, e2019MS001978, https://doi.org/10.1029/2019MS001978, 2020.

Buchard, V., Randles, C. A., da Silva, A. M., Darmenov, A., Colarco, P. R., Govindaraju, R., Ferrare, R., Hair, J., Beyersdorf, A. J., Ziemba, L. D., and Yu, H.: The MERRA-2 Aerosol Reanalysis, 1980 Onward. Part II: Evaluation and Case Studies, J. Climate, 30, 6851–6872, https://doi.org/10.1175/JCLI-D-16-0613.1, 2017.

Capelle, V., Chédin, A., Pondrom, M., Crevoisier, C., Armante, R., Crepeau, L., and Scott, N. A.: Infrared dust aerosol optical depth retrieved daily from IASI and comparison with

https://doi.org/10.5194/egusphere-2026-4322
Preprint. Discussion started: 17 August 2026

AERONET over the period 2007–2016, Remote Sens Environ, 206, 15-32, https://doi.org/10.1016/j.rse.2017.12.008, 2018.

Cakmur, R. V., Miller, R. L., Perlwitz, J., Geogdzhayev, I. V., Ginoux, P., Koch, D., Kohfeld, K. E., Tegen, I., and Zender, C. S.: Constraining the magnitude of the global dust cycle by minimizing the difference between a model and observations, J Geophys Res Atmospheres, 111, https://doi.org/10.1029/2005JD005791, 2006.

Castellanos P., P. Colarco, W. R. Espinosa, S. D. Guzewich, R. C. Levy, R. L. Miller, M. Chin, R. A. Kahn, O. Kemppinen, H. Moosmüller, E. P. Nowottnick, A. Rocha-Lima, M. D. Smith, J. E. Yorks and H. Yu. 2024. "Mineral dust optical properties for remote sensing and global modeling: A review.", Remote Sensing of Environment, 303 113982 [10.1016/j.rse.2023.113982]

Checa-Garcia, R., Balkanski, Y., Albani, S., Bergman, T., Carslaw, K., Cozic, A., Dearden, C., Marticorena, B., Michou, M., van Noije, T., Nabat, P., O'Connor, F. M., Olivié, D., Prospero, J. M., Le Sager, P., Schulz, M., and Scott, C.: Evaluation of natural aerosols in CRESCENDO Earth system models (ESMs): mineral dust, Atmos. Chem. Phys., 21, 10295-10335, https://doi.org/10.5194/acp-21-10295-2021, 2021.

Chen, C., Dubovik, O., Henze, D. K., Chin, M., Lapyonok, T., Schuster, G. L., Ducos, F., Fuertes, D., Litvinov, P., Li, L., Lopatin, A., Hu, Q., and Torres, B.: Constraining global aerosol emissions using POLDER/PARASOL satellite remote sensing observations, Atmos. Chem. Phys., 19, 14585–14606, https://doi.org/10.5194/acp-19-14585-2019, 2019.

Cheng, T., Peng, Y., Feichter, J., and Tegen, I.: An improvement on the dust emission scheme in the global aerosol-climate model ECHAM5-HAM, Atmos. Chem. Phys., 8, 1105–1117, https://doi.org/10.5194/acp-8-1105-2008, 2008.

Chin, M., Ginoux, P., Kinne, S., Torres, O., Holben, B. N., Duncan, B. N., Martin, R. V., Logan, J. A., Higurashi, A., and Nakajima, T.: Tropospheric Aerosol Optical Thickness from the GOCART Model and Comparisons with Satellite and Sun Photometer Measurements, J Atmos Sci, 59, 461-483, https://doi.org/10.1175/1520-0469(2002)059<0461:TAOTFT>2.0.CO;2, 2002.

Colarco, P., da Silva, A., Chin, M., and Diehl, T.: Online simulations of global aerosol distributions in the NASA GEOS-4 model and comparisons to satellite and ground-based aerosol optical depth, J Geophys Res Atmospheres, 115, https://doi.org/10.1029/2009JD012820, 2010.

Cornwell, G. C., Xiao, H., Berg, L. K., and Burrows, S. M.: Simulated dust transport in the convective boundary layer, Journal of Geophysical Research: Atmospheres, 126, https://doi.org/10.1029/2020jd033429, 2021.

Di Biagio, C., Balkanski, Y., Albani, S., Boucher, O., and Formenti, P.: Direct Radiative Effect by Mineral Dust Aerosols Constrained by New Microphysical and Spectral Optical Data, Geophys Res Lett, 47, e2019GL086186, https://doi.org/10.1029/2019GL086186, 2020.

Dubovik, O., Sinyuk, A., Lapyonok, T., Holben, B. N., Mishchenko, M., Yang, P., Eck, T. F., Volten, H., Muñoz, O., Veihelmann, B., van der Zande, W. J., Leon, J.-F., Sorokin, M., and Slutsker, I.: Application of spheroid models to account for aerosol particle nonsphericity in remote sensing of desert dust, J Geophys Res Atmospheres, 111, https://doi.org/10.1029/2005JD006619, 2006.

Drakaki, E., Amiridis, V., Tsekeri, A., Gkikas, A., Proestakis, E., Mallios, S., Solomos, S., Spyrou, C., Marinou, E., Ryder, C. L., Bouris, D., and Katsafados, P.: Modeling coarse and giant desert dust particles, Atmos. Chem. Phys., 22, 12727-12748,

https://doi.org/10.5194/egusphere-2026-4322
Preprint. Discussion started: 17 August 2026

https://doi.org/10.5194/acp-22-12727-2022, 2022.

Evan, A. T., Dunion, J., Foley, J. A., Heidinger, A. K., and Velden, C. S.: New evidence for a relationship between Atlantic tropical cyclone activity and African dust outbreaks, Geophys Res Lett, 33, 2006.

Ferrare, R., Hair, J., Hostetler, C., Shingler, T., Burton, S. P., Fenn, M., Clayton, M., Scarino, A. J., Harper, D., Seaman, S., Cook, A., Crosbie, E., Winstead, E., Ziemba, L., Thornhill, L., Robinson, C., Moore, R., Vaughan, M., Sorooshian, A., Schlosser, J. S., Liu, H., Zhang, B., Diskin, G., DiGangi, J., Nowak, J., Choi, Y., Zuidema, P., and Chellappan, S.: Airborne HSRL-2 measurements of elevated aerosol depolarization associated with non-spherical sea salt, Frontiers in Remote Sensing, Volume 4 - 2023, https://doi.org/10.3389/frsen.2023.1143944, 2023.

Formenti, P., Mbemba Kabuiku, L., Chiapello, I., Ducos, F., Dulac, F., and Tanré, D.: Aerosol optical properties derived from POLDER-3/PARASOL (2005–2013) over the western Mediterranean Sea – Part 1: Quality assessment with AERONET and in situ airborne observations, Atmos. Meas. Tech., 11, 6761–6784, https://doi.org/10.5194/amt-11-6761-2018, 2018.

Friese, C. A., van Hateren, J. A., Vogt, C., Fischer, G., and Stuut, J. B. W.: Seasonal provenance changes in present-day Saharan dust collected in and off Mauritania, Atmos. Chem. Phys., 17, 10163-10193, https://doi.org/10.5194/acp-17-10163-2017, 2017.

Garay, M. J., Witek, M. L., Kahn, R. A., Seidel, F. C., Limbacher, J. A., Bull, M. A., Diner, D. J., Hansen, E. G., Kalashnikova, O. V., Lee, H., Nastan, A. M., and Yu, Y.: Introducing the 4.4 km spatial resolution Multi-Angle Imaging SpectroRadiometer (MISR) aerosol product, Atmos. Meas. Tech., 13, 593-628, https://doi.org/10.5194/amt-13-593-2020, 2020.

Gasteiger, J., Groß, S., Sauer, D., Haarig, M., Ansmann, A., and Weinzierl, B.: Particle settling and vertical mixing in the Saharan Air Layer as seen from an integrated model, lidar, and in situ perspective, Atmos. Chem. Phys., 17, 297-311, https://doi.org/10.5194/acp-17-297-2017, 2017.

Gelaro, R., McCarty, W., Suárez, M. J., Todling, R., Molod, A., Takacs, L., Randles, C. A., Darmenov, A., Bosilovich, M. G., Reichle, R., Wargan, K., Coy, L., Cullather, R., Draper, C., Akella, S., Buchard, V., Conaty, A., da Silva, A. M., Gu, W., Kim, G.-K., Koster, R., Lucchesi, R., Merkova, D., Nielsen, J. E., Partyka, G., Pawson, S., Putman, W., Rienecker, M., Schubert, S. D., Sienkiewicz, M., and Zhao, B.: The Modern-Era Retrospective Analysis for Research and Applications, Version 2 (MERRA-2), J. Climate, 30, 5419-5454, https://doi.org/10.1175/JCLI-D-16-0758.1, 2017.

Gillette, D. A.: A wind tunnel simulation of the erosion of soil: Effect of soil texture, sandblasting, wind speed, and soil consolidation on dust production, Atmos Environ, 12, 1735–1743, https://doi.org/10.1016/0004-6981(78)90322-0, 1978.

Ginoux, P., Chin, M., Tegen, I., Prospero, J. M., Holben, B., Dubovik, O., and Lin, S.-J.: Sources and distributions of dust aerosols simulated with the GOCART model, J Geophys Res Atmospheres, 106, 20255–20273, https://doi.org/10.1029/2000JD000053, 2001.

Ginoux, P.: Effects of nonsphericity on mineral dust modeling, J Geophys Res Atmospheres, 108, https://doi.org/10.1029/2002JD002516, 2003.

Ginoux, P., Prospero, J. M., Gill, T. E., Hsu, N. C., and Zhao, M.: Global-scale attribution of anthropogenic and natural dust sources and their emission rates based on MODIS Deep Blue aerosol products, Reviews of Geophysics, 50, https://doi.org/10.1029/2012RG000388, 2012.

Gliß, J., Mortier, A., Schulz, M., Andrews, E., Balkanski, Y., Bauer, S. E., Benedictow, A. M.

https://doi.org/10.5194/egusphere-2026-4322
Preprint. Discussion started: 17 August 2026

K., Bian, H., Checa-Garcia, R., Chin, M., Ginoux, P., Griesfeller, J. J., Heckel, A., Kipling, Z., Kirkevåg, A., Kokkola, H., Laj, P., Le Sager, P., Lund, M. T., Lund Myhre, C., Matsui, H., Myhre, G., Neubauer, D., van Noije, T., North, P., Olivié, D. J. L., Rémy, S., Sogacheva, L., Takemura, T., Tsigaridis, K., and Tsyro, S. G.: AeroCom phase III multi-model evaluation of the aerosol life cycle and optical properties using ground- and space-based remote sensing as well as surface in situ observations, Atmos. Chem. Phys., 21, 87-128, https://doi.org/10.5194/acp-21-87-2021, 2021.

Gonçalves Ageitos, M., Obiso, V., Miller, R. L., Jorba, O., Klose, M., Dawson, M., Balkanski, Y., Perlwitz, J., Basart, S., Di Tomaso, E., Escribano, J., Macchia, F., Montané, G., Mahowald, N. M., Green, R. O., Thompson, D. R., and Pérez García-Pando, C.: Modeling dust mineralogical composition: sensitivity to soil mineralogy atlases and their expected climate impacts, Atmos. Chem. Phys., 23, 8623-8657, https://doi.org/10.5194/acp-23-8623-2023, 2023.

Gong, S. L., Zhang, X. Y., Zhao, T. L., McKendry, I. G., Jaffe, D. A., and Lu, N. M.: Characterization of soil dust aerosol in China and its transport and distribution during 2001 ACE-Asia: 2. Model simulation and validation, J Geophys Res Atmospheres, 108, https://doi.org/10.1029/2002JD002633, 2003.

Grini, A., Myhre, G., Zender, C. S., and Isaksen, I. S. A.: Model simulations of dust sources and transport in the global atmosphere: Effects of soil erodibility and wind speed variability, J Geophys Res Atmospheres, 110, https://doi.org/10.1029/2004JD005037, 2005.

Huang, Y., Liu, C., Yao, B., Yin, Y., and Bi, L.: Scattering matrices of mineral dust aerosols: a refinement of the refractive index impact, Atmospheric Chemistry & Physics, 20, 2020.

Heinold, B., Tegen, I., Esselborn, M., Kandler, K., Knippertz, P., Müller, D., Schladitz, A., Sodemann, H., Tuch, T., Wiegner, M., and Amiridis, V.: Regional Saharan dust modelling during the SAMUM 2006 campaign, Tellus B, 61, 307–324, https://doi.org/10.1111/j.1600-0889.2008.00387.x, 2009.

Holben, B. N., Eck, T. F., Slutsker, I., Tanré, D., Buis, J. P., Setzer, A., Vermote, E., Reagan, J. A., Kaufman, Y. J., Nakajima, T., Lavenu, F., Jankowiak, I., and Smirnov, A.: AERONET—A Federated Instrument Network and Data Archive for Aerosol Characterization, Remote Sens Environ, 66, 1–16, https://doi.org/10.1016/S0034-4257(98)00031-5, 1998.

Huneeus, N., Schulz, M., Balkanski, Y., Griesfeller, J., Prospero, J., Kinne, S., Bauer, S., Boucher, O., Chin, M., Dentener, F., Diehl, T., Easter, R., Fillmore, D., Ghan, S., Ginoux, P., Grini, A., Horowitz, L., Koch, D., Krol, M. C., Landing, W., Liu, X., Mahowald, N., Miller, R., Morcrette, J. J., Myhre, G., Penner, J., Perlwitz, J., Stier, P., Takemura, T., and Zender, C. S.: Global dust model intercomparison in AeroCom phase I, Atmos. Chem. Phys., 11, 7781-7816, https://doi.org/10.5194/acp-11-7781-2011, 2011.

Inness, A., Ades, M., Agustí-Panareda, A., Barré, J., Benedictow, A., Blechschmidt, A.-M., Dominguez, J. J., Engelen, R., Eskes, H., Flemming, J., Huijnen, V., Jones, L., Kipling, Z., Massart, S., Parrington, M., Peuch, V.-H., Razinger, M., Remy, S., Schulz, M., and Suttie, M.: The CAMS reanalysis of atmospheric composition, Atmos. Chem. Phys., 19, 3515-3556, https://doi.org/10.5194/acp-19-3515-2019, 2019.

Kahn, R. A. and Gaitley, B. J.: An analysis of global aerosol type as retrieved by MISR, J Geophys Res Atmospheres, 120, 4248-4281, https://doi.org/10.1002/2015JD023322, 2015.

Kahn, R. A., Gaitley, B. J., Garay, M. J., Diner, D. J., Eck, T. F., Smirnov, A., and Holben, B. N.: Multiangle Imaging SpectroRadiometer global aerosol product assessment by comparison with the Aerosol Robotic Network, J Geophys Res Atmospheres, 115,

https://doi.org/10.5194/egusphere-2026-4322
Preprint. Discussion started: 17 August 2026

https://doi.org/10.1029/2010JD014601, 2010.

Karydis, V. A., Kumar, P., Barahona, D., Sokolik, I. N., and Nenes, A.: On the effect of dust particles on global cloud condensation nuclei and cloud droplet number, J Geophys Res Atmospheres, 116, https://doi.org/10.1029/2011JD016283, 2011.

Kaufman, Y. J., Koren, I., Remer, L. A., Tanre, D., Ginoux, P., and Fan, S.: Dust transport and deposition observed from the Terra-Moderate Resolution Imaging Spectroradiometer (MODIS) spacecraft over the Atlantic ocean, Journal of Geophysical Research-Atmospheres, 110, https://doi.org/10.1029/2003jd004436, 2005.

Kim, D., Chin, M., Yu, H., Pan, X., Bian, H., Tan, Q., Kahn, R. A., Tsigaridis, K., Bauer, S. E., Takemura, T., Pozzoli, L., Bellouin, N., and Schulz, M.: Asian and Trans-Pacific Dust: A Multimodel and Multiremote Sensing Observation Analysis, J Geophys Res Atmospheres, 124, 13534-13559, https://doi.org/10.1029/2019JD030822, 2019.

Kim, D., Chin, M., Yu, H., Diehl, T., Tan, Q., Kahn, R. A., Tsigaridis, K., Bauer, S. E., Takemura, T., Pozzoli, L., Bellouin, N., Schulz, M., Peyridieu, S., Chédin, A., and Koffi, B.: Sources, sinks, and transatlantic transport of North African dust aerosol: A multimodel analysis and comparison with remote sensing data, J Geophys Res Atmospheres, 119, 6259-6277, https://doi.org/10.1002/2013JD021099, 2014.

Kim, D., Chin, M., Bian, H., Tan, Q., Brown, M. E., Zheng, T., You, R., Diehl, T., Ginoux, P., and Kuber, T.: The effect of the dynamic surface bareness on dust source function, emission, and distribution, J Geophys Res Atmospheres, 118, 871–886, https://doi.org/10.1029/2012JD017907, 2013.

Kirkevåg, A., Grini, A., Olivié, D., Seland, Ø., Alterskjær, K., Hummel, M., Karset, I. H. H., Lewinschal, A., Liu, X., Makkonen, R., Bethke, I., Griesfeller, J., Schulz, M., and Iversen, T.: A production-tagged aerosol module for Earth system models, OsloAero5.3 – extensions and updates for CAM5.3-Oslo, Geosci. Model Dev., 11, 3945-3982, https://doi.org/10.5194/gmd-11-3945-2018, 2018.

Koffi, B., Schulz, M., Bréon, F. M., Griesfeller, J., Winker, D. M., Balkanski, Y., Bauer, S. E., Berntsen, T. K., Chin, M., Collins, W. D., Dentener, F., Diehl, T., Easter, R. C., Ghan, S. J., Ginoux, P., Gong, S., Horowitz, L. W., Iversen, T., Kirkevåg, A., Koch, D., Krol, M., Myhre, G., Stier, P., and Takemura, T.: Application of the CALIOP Layer Product to Evaluate the Vertical Distribution of Aerosols Estimated by Global Models: AeroCom Phase I Results, Journal of Geophysical Research Atmospheres, 117, https://doi.org/10.1029/2011jd016858, 2012.

Koffi, B., Schulz, M., Bréon, F. M., Dentener, F., Steensen, B. M., Griesfeller, J., Winker, D. M., Balkanski, Y., Bauer, S. E., Bellouin, N., Berntsen, T. K., Bian, H., Chin, M., Diehl, T., Easter, R. C., Ghan, S. J., Hauglustaine, D., Iversen, T., Kirkevåg, A., Liu, X., Lohmann, U., Myhre, G., Rasch, P., Seland, Ø., Skeie, R. B., Steenrod, S. D., Stier, P., Tackett, J. L., Takemura, T., Tsigaridis, K., Vuolo, M. R., Yoon, J. H., and Zhang, K.: Evaluation of the Aerosol Vertical Distribution in Global Aerosol Models Through Comparison Against CALIOP Measurements: AeroCom Phase II Results, Journal of Geophysical Research Atmospheres, 121, 7254-7283, https://doi.org/10.1002/2015jd024639, 2016.

Kok, J. F., Storelvmo, T., Karydis, V. A., Adebiyi, A. A., Mahowald, N. M., Evan, A. T., He, C., and Leung, D. M.: Mineral dust aerosol impacts on global climate and climate change, Nature Reviews Earth & Environment, 4, 71-86, https://doi.org/10.1038/s43017-022-00379-5, 2023.

Kok, J. F., Adebiyi, A. A., Albani, S., Balkanski, Y., Checa-Garcia, R., Chin, M., Colarco, P. R., Hamilton, D. S., Huang, Y., Ito, A., Klose, M., Leung, D. M., Li, L., Mahowald, N. M.,

https://doi.org/10.5194/egusphere-2026-4322
Preprint. Discussion started: 17 August 2026

Miller, R. L., Obiso, V., Pérez García-Pando, C., Rocha-Lima, A., Wan, J. S., and Whicker, C. A.: Improved representation of the global dust cycle using observational constraints on dust properties and abundance, Atmos. Chem. Phys., 21, 8127-8167, https://doi.org/10.5194/acp-21-8127-2021, 2021.

Kok, J. F.: A scaling theory for the size distribution of emitted dust aerosols suggests climate models underestimate the size of the global dust cycle, Proc Natl Acad Sci USA, 108, 1016–1021, https://doi.org/10.1073/pnas.1014798108, 2011.

Kok, J. F., Mahowald, N. M., Fratini, G., Gillies, J. A., Ishizuka, M., Leys, J. F., Mikami, M., Park, M.-S., Park, S.-U., Van Pelt, R. S., and Zobeck, T. M.: An improved dust emission model – Part 1: Model description and comparison against measurements, Atmos. Chem. Phys., 14, 13023–13041, https://doi.org/10.5194/acp-14-13023-2014, 2014.

Kok, J. F., Ridley, D. A., Zhou, Q., Miller, R. L., Zhao, C., Heald, C. L., Ward, D. S., Albani, S., and Haustein, K.: Smaller desert dust cooling effect estimated from analysis of dust size and abundance, Nat Geosci, 10, 274–278, https://doi.org/10.1038/ngeo2912, 2017.

Kokkola, H., Kühn, T., Laakso, A., Bergman, T., Lehtinen, K. E. J., Mielonen, T., Arola, A., Stadtler, S., Korhonen, H., Ferrachat, S., Lohmann, U., Neubauer, D., Tegen, I., Siegenthaler-Le Drian, C., Schultz, M. G., Bey, I., Stier, P., Daskalakis, N., Heald, C. L., and Romakkaniemi, S.: SALSA2.0: The sectional aerosol module of the aerosol–chemistry–climate model ECHAM6.3.0-HAM2.3-MOZ1.0, Geosci. Model Dev., 11, 3833-3863, https://doi.org/10.5194/gmd-11-3833-2018, 2018.

Korte, L. F., Brummer, G. J. A., van der Does, M., Guerreiro, C. V., Hennekam, R., van Hateren, J. A., Jong, D., Munday, C. I., Schouten, S., and Stuut, J. B. W.: Downward particle fluxes of biogenic matter and Saharan dust across the equatorial North Atlantic, Atmos. Chem. Phys., 17, 6023-6040, https://doi.org/10.5194/acp-17-6023-2017, 2017.

Li, L., Derimian, Y., Chen, C., Zhang, X., Che, H., Schuster, G. L., Fuertes, D., Litvinov, P., Lapyonok, T., Lopatin, A., Matar, C., Ducos, F., Karol, Y., Torres, B., Gui, K., Zheng, Y., Liang, Y., Lei, Y., Zhu, J., Zhang, L., Zhong, J., Zhang, X., and Dubovik, O.: Climatology of aerosol component concentrations derived from multi-angular polarimetric POLDER-3 observations using GRASP algorithm, Earth Syst. Sci. Data, 14, 3439–3469, https://doi.org/10.5194/essd-14-3439-2022, 2022.

Lian, S., Zhou, L., Murphy, D. M., Froyd, K. D., Toon, O. B., and Yu, P.: Global Distribution of Asian, Middle Eastern, and North African Dust Simulated by CESM1/CARMA, Atmos Chem Phys, 22, 13659-13676, https://doi.org/10.5194/acp-22-13659-2022, 2022.

Lund, M. T., Myhre, G., Haslerud, A. S., Skeie, R. B., Griesfeller, J., Platt, S. M., Kumar, R., Myhre, C. L., and Schulz, M.: Concentrations and radiative forcing of anthropogenic aerosols from 1750 to 2014 simulated with the Oslo CTM3 and CEDS emission inventory, Geosci. Model Dev., 11, 4909-4931, https://doi.org/10.5194/gmd-11-4909-2018, 2018.

Maher, B. A., Prospero, J. M., Mackie, D., Gaiero, D., Hesse, P. P., and Balkanski, Y.: Global connections between aeolian dust, climate and ocean biogeochemistry at the present day and at the last glacial maximum, Earth-Science Reviews, 99, 61-97, https://doi.org/10.1016/j.earscirev.2009.12.001, 2010.

Mallios, S. A., Daskalopoulou, V., and Amiridis, V.: Modeling of the electrical interaction between desert dust particles and the Earth's atmosphere, Journal of Aerosol Science, 165, 106044, https://doi.org/10.1016/j.jaerosci.2022.106044, 2022.

Maring, H., Savoie, D. L., Izaguirre, M. A., Custals, L., and Reid, J. S.: Mineral dust aerosol size distribution change during atmospheric transport, J Geophys Res Atmospheres, 108,

https://doi.org/10.5194/egusphere-2026-4322
Preprint. Discussion started: 17 August 2026

https://doi.org/10.1029/2002JD002536, 2003.

Marticorena, B. and Bergametti, G.: Modeling the atmospheric dust cycle: 1. Design of a soil-derived dust emission scheme, J Geophys Res Atmospheres, 100, 16415–16430, https://doi.org/10.1029/95JD00690, 1995.

Matsui, H.: Development of a global aerosol model using a two-dimensional sectional method: 1. Model design, Journal of Advances in Modeling Earth Systems, 9, 1921-1947, https://doi.org/10.1002/2017MS000936, 2017.

Matsui, H. and Mahowald, N.: Development of a global aerosol model using a two-dimensional sectional method: 2. Evaluation and sensitivity simulations, Journal of Advances in Modeling Earth Systems, 9, 1887-1920, https://doi.org/10.1002/2017MS000937, 2017.

Meng, J., Huang, Y., Leung, D. M., Li, L., Adebiyi, A. A., Ryder, C. L., Mahowald, N. M., and Kok, J. F.: Improved Parameterization for the Size Distribution of Emitted Dust Aerosols Reduces Model Underestimation of Super Coarse Dust, Geophys Res Lett, 49, e2021GL097287, https://doi.org/10.1029/2021GL097287, 2022.

Miller, R. L., Tegen, I., and Perlwitz, J.: Surface radiative forcing by soil dust aerosols and the hydrologic cycle, J Geophys Res Atmospheres, 109, https://doi.org/10.1029/2003JD004085, 2004.

Morcrette, J.-J., Boucher, O., Jones, L., Salmond, D., Bechtold, P., Beljaars, A., Benedetti, A., Bonet, A., Kaiser, J. W., Razinger, M., Schulz, M., Serrar, S., Simmons, A. J., Sofiev, M., Suttie, M., Tompkins, A. M., and Untch, A.: Aerosol analysis and forecast in the European Centre for Medium-Range Weather Forecasts Integrated Forecast System: Forward modeling, J. Geophys. Res., 114, D06206, https://doi.org/10.1029/2008JD011235, 2009.

Morton, P. L., Landing, W. M., Hsu, S.-C., Milne, A., Aguilar-Islas, A. M., Baker, A. R., Bowie, A. R., Buck, C. S., Gao, Y., Gichuki, S., Hastings, M. G., Johansen, A. M., Losno, R., Maishi, C., Nishioka, J., Sarin, M. M., Sarthou, G., Schmitt, H. R., Serno, S., Sohst, B., Vink, S., and Wuttig, K.: Methods for the sampling and analysis of marine aerosols: Results from the 2008 GEOTRACES aerosol intercalibration experiment, Limnol. Oceanogr. Methods, 11, 62-78, https://doi.org/10.4319/lom.2013.11.62, 2013.

Nousiainen, T.: Optical modeling of mineral dust particles: A review, J Quant Spectrosc Ra, 110, 1261–1279, https://doi.org/10.1016/j.jqsrt.2009.03.002, 2009.

Nowottnick E., P. R. Colarco, A. M. Da Silva, D. L. Hlavka and M. J. Mcgill. 2011. "The fate of Saharan dust across the Atlantic and implications for a Central American dust barrier.", Atmos. Chem. Phys., 11 (16): 8415-8431 [10.5194/acp-11-8415-2011]

Obiso, V., Gonçalves Ageitos, M., Pérez García-Pando, C., Schuster, G. L., Bauer, S. E., Di Biagio, C., Formenti, P., Perlwitz, J. P., Tsigaridis, K., and Miller, R. L.: Global impact of dust particle non-sphericity on the longwave radiative effect, Atmos. Chem. Phys., 2026.

O'Neill, N. T., Eck, T. F., Smirnov, A., Holben, B. N., and Thulasiraman, S.: Spectral discrimination of coarse and fine mode optical depth, J Geophys Res Atmospheres, 108, https://doi.org/10.1029/2002JD002975, 2003.

Osborne, S. R., Baran, A. J., Johnson, B. T., Haywood, J. M., Hesse, E., and Newman, S.: Short-wave and long-wave radiative properties of Saharan dust aerosol, Quarterly Journal of the Royal Meteorological Society, 137, 1149-1167, https://doi.org/10.1002/qj.771, 2011.

Papetta, A., Formenti, P., Pikridas, M., and Sciare, J.: Synthesis of airborne and ground-based observations of dust optical properties over the eastern Atlantic, Atmos. Chem. Phys., 2026.

Proestakis, E., Amiridis, V., García-Pando, C. P., Tsyro, S., Griesfeller, J., Gkikas, A., Georgiou, T., Ageitos, M. G., Escribano, J., Myriokefalitakis, S., Masso, E. B., Di Tomaso, E., Basart,

https://doi.org/10.5194/egusphere-2026-4322
Preprint. Discussion started: 17 August 2026

S., Stuut, J. B. W., and Benedetti, A.: Quantifying dust deposition over the Atlantic Ocean, Earth Syst. Sci. Data, 17, 4351-4395, https://doi.org/10.5194/essd-17-4351-2025, 2025.

Prospero, J. M., Collard, F.-X., Molinié, J., and Jeannot, A.: Characterizing the annual cycle of African dust transport to the Caribbean Basin and South America and its impact on the environment and air quality, Global Biogeochemical Cycles, 28, 757-773, https://doi.org/10.1002/2013GB004802, 2014.

Pu, B. and Ginoux, P.: How reliable are CMIP5 models in simulating dust optical depth?, Atmos. Chem. Phys., 18, 12491-12510, https://doi.org/10.5194/acp-18-12491-2018, 2018.

Ratcliffe, N. G., Ryder, C. L., Bellouin, N., Woodward, S., Jones, A., Johnson, B., Wieland, L. M., Dollner, M., Gasteiger, J., and Weinzierl, B.: Long-range transport of coarse mineral dust: an evaluation of the Met Office Unified Model against aircraft observations, Atmos. Chem. Phys., 24, 12161-12181, https://doi.org/10.5194/acp-24-12161-2024, 2024.

Remer, L. A.: Dust, fertilization and sources, Environmental Research Letters, 1, 011001, https://doi.org/10.1088/1748-9326/1/1/011001, 2006.

Renard, J. B., Dulac, F., Durand, P., Bourgeois, Q., Denjean, C., Vignelles, D., Couté, B., Jeannot, M., Verdier, N., and Mallet, M.: In situ measurements of desert dust particles above the western Mediterranean Sea with the balloon-borne Light Optical Aerosol Counter/sizer (LOAC) during the ChArMEx campaign of summer 2013, Atmospheric Chemistry and Physics, 18, 3677–3699, https://doi.org/10.5194/acp-18-3677-2018, 2018.

Rémy, S., Kipling, Z., Huijnen, V., Flemming, J., Nabat, P., Michou, M., Ades, M., Engelen, R., and Peuch, V. H.: Description and evaluation of the tropospheric aerosol scheme in the Integrated Forecasting System (IFS-AER, cycle 47R1) of ECMWF, Geosci. Model Dev., 15, 4881-4912, https://doi.org/10.5194/gmd-15-4881-2022, 2022.

Rémy, S., Kipling, Z., Flemming, J., Boucher, O., Nabat, P., Michou, M., Bozzo, A., Ades, M., Huijnen, V., Benedetti, A., Engelen, R., Peuch, V. H., and Morcrette, J. J.: Description and evaluation of the tropospheric aerosol scheme in the European Centre for Medium-Range Weather Forecasts (ECMWF) Integrated Forecasting System (IFS-AER, cycle 45R1), Geosci. Model Dev., 12, 4627-4659, https://doi.org/10.5194/gmd-12-4627-2019, 2019.

Rodakoviski, R., Kok, J., and Chamecki, M.: Dust Settling From Turbulent Layers in the Free Troposphere: Implications for the Saharan Air Layer, Journal of Geophysical Research: Atmospheres, 128, https://doi.org/10.1029/2022JD037724, 2023.

Ryder, C. L., Highwood, E. J., Lai, T. M., Sodemann, H., and Marsham, J. H.: Impact of atmospheric transport on the evolution of microphysical and optical properties of Saharan dust, Geophys Res Lett, 40, 2433-2438, https://doi.org/10.1002/grl.50482, 2013a.

Ryder, C. L., Highwood, E. J., Walser, A., Seibert, P., Philipp, A., and Weinzierl, B.: Coarse and giant particles are ubiquitous in Saharan dust export regions and are radiatively significant over the Sahara, Atmos. Chem. Phys., 19, 15353-15376, https://doi.org/10.5194/acp-19-15353-2019, 2019.

Ryder, C. L., Highwood, E. J., Rosenberg, P. D., Trembath, J., Brooke, J. K., Bart, M., Dean, A., Crosier, J., Dorsey, J., Brindley, H., Banks, J., Marsham, J. H., McQuaid, J. B., Sodemann, H., and Washington, R.: Optical properties of Saharan dust aerosol and contribution from the coarse mode as measured during the Fennec 2011 aircraft campaign, Atmos Chem Phys, 13, 303-325, https://doi.org/10.5194/acp-13-303-2013, 2013b.

Ryder, C. L., Marenco, F., Brooke, J. K., Estelles, V., Cotton, R., Formenti, P., McQuaid, J. B., Price, H. C., Liu, D., Ausset, P., Rosenberg, P. D., Taylor, J. W., Choularton, T., Bower, K., Coe, H., Gallagher, M., Crosier, J., Lloyd, G., Highwood, E. J., and Murray, B. J.: Coarse-

https://doi.org/10.5194/egusphere-2026-4322
Preprint. Discussion started: 17 August 2026

mode mineral dust size distributions, composition and optical properties from AER-D aircraft measurements over the tropical eastern Atlantic, Atmos. Chem. Phys., 18, 17225-17257, https://doi.org/10.5194/acp-18-17225-2018, 2018.

Shao, Y., Wyrwoll, K.-H., Chappell, A., Huang, J., Lin, Z., McTainsh, G. H., Mikami, M., Tanaka, T. Y., Wang, X., and Yoon, S.: Dust cycle: An emerging core theme in Earth system science, Aeolian Res, 2, 181-204, 2011.

Song, Q., Zhang, Z., Yu, H., Ginoux, P., and Shen, J.: Global Dust Optical Depth Climatology Derived from CALIOP and MODIS Aerosol Retrievals on Decadal Time Scales: Regional and Interannual Variability, Atmos. Chem. Phys. Discuss., 2021, 1-57, https://doi.org/10.5194/acp-2021-1, 2021.

SWAP, R., GARSTANG, M., GRECO, S., TALBOT, R., and KÅLLBERG, P.: Saharan dust in the Amazon Basin, Tellus B, 44, 133-149, https://doi.org/10.1034/j.1600-0889.1992.t01-1-00005.x, 1992.

Takemura, T., Nakajima, T., Higurashi, A., Ohta, S., and Sugimoto, N.: Aerosol distributions and radiative forcing over the Asian Pacific region simulated by Spectral Radiation-Transport Model for Aerosol Species (SPRINTARS), J Geophys Res Atmospheres, 108, https://doi.org/10.1029/2002JD003210, 2003.

Tegen, I., Harrison, S. P., Kohfeld, K., Prentice, I. C., Coe, M., and Heimann, M.: Impact of vegetation and preferential source areas on global dust aerosol: Results from a model study, J Geophys Res Atmospheres, 107, https://doi.org/10.1029/2001JD000963, 2002.

Tegen, I., Neubauer, D., Ferrachat, S., Siegenthaler-Le Drian, C., Bey, I., Schutgens, N., Stier, P., Watson-Parris, D., Stanelle, T., Schmidt, H., Rast, S., Kokkola, H., Schultz, M., Schroeder, S., Daskalakis, N., Barthel, S., Heinold, B., and Lohmann, U.: The global aerosol–climate model ECHAM6.3–HAM2.3 – Part 1: Aerosol evaluation, Geosci. Model Dev., 12, 1643-1677, https://doi.org/10.5194/gmd-12-1643-2019, 2019.

Toth III, J. R., Rajupet, S., Squire, H., Volbers, B., Zhou, J., Xie, L., Sankaran, R. M., and Lacks, D. J.: Electrostatic forces alter particle size distributions in atmospheric dust, Atmos. Chem. Phys., 20, 3181–3190, https://doi.org/10.5194/acp-20-3181-2020, 2020.

Textor, C., Schulz, M., Guibert, S., Kinne, S., Balkanski, Y., Bauer, S., Berntsen, T., Berglen, T., Boucher, O., Chin, M., Dentener, F., Diehl, T., Easter, R., Feichter, H., Fillmore, D., Ghan, S., Ginoux, P., Gong, S., Grini, A., Hendricks, J., Horowitz, L., Huang, P., Isaksen, I., Iversen, I., Kloster, S., Koch, D., Kirkev˚ag, A., Kristjansson, J. E., Krol, M., Lauer, A., Lamarque, J. F., Liu, X., Montanaro, V., Myhre, G., Penner, J., Pitari, G., Reddy, S., Seland, Ø., Stier, P., Takemura, T., and Tie, X.: Analysis and quantification of the diversities of aerosol life cycles within AeroCom, Atmos. Chem. Phys., 6, 1777–1813, https://doi.org/10.5194/acp-6-1777-2006, 2006.

Ukhov, A., Ahmadov, R., Grell, G., and Stenchikov, G.: Improving dust simulations in WRF-Chem v4.1.3 coupled with the GOCART aerosol module, Geosci. Model Dev., 14, 473-493, https://doi.org/10.5194/gmd-14-473-2021, 2021.

van der Does, M., Knippertz, P., Zschenderlein, P., Giles Harrison, R., and Stuut, J.-B. W.: The mysterious long-range transport of giant mineral dust particles, Sci Adv, 4, eaau2768, doi:https://doi.org/10.1126/sciadv.aau2768, 2018.

van Noije, T., Bergman, T., Le Sager, P., O'Donnell, D., Makkonen, R., Gonçalves-Ageitos, M., Döscher, R., Fladrich, U., von Hardenberg, J., Keskinen, J. P., Korhonen, H., Laakso, A., Myriokefalitakis, S., Ollinaho, P., Pérez García-Pando, C., Reerink, T., Schrödner, R., Wyser, K., and Yang, S.: EC-Earth3-AerChem: a global climate model with interactive aerosols and

https://doi.org/10.5194/egusphere-2026-4322
Preprint. Discussion started: 17 August 2026

atmospheric chemistry participating in CMIP6, Geosci. Model Dev., 14, 5637-5668, https://doi.org/10.5194/gmd-14-5637-2021, 2021.

Westberry, T. K., Shi, Y. R., Yu, H., Behrenfeld, M. J., and Remer, L. A.: Satellite-Detected Ocean Ecosystem Response to Volcanic Eruptions in the Subarctic Northeast Pacific Ocean, Geophys Res Lett, 49, e2021GL097000, https://doi.org/10.1029/2021GL097000, 2022.

Wu, M., Liu, X., Yu, H., Wang, H., Shi, Y., Yang, K., Darmenov, A., Wu, C., Wang, Z., Luo, T., Feng, Y., and Ke, Z.: Understanding processes that control dust spatial distributions with global climate models and satellite observations, Atmos. Chem. Phys., 20, 13835-13855, https://doi.org/10.5194/acp-20-13835-2020, 2020.

Xi, X., Wang, J., Lu, Z., Sayer, A. M., Lee, J., Levy, R. C., Wang, Y., Lyapustin, A., Liu, H., Laszlo, I., Ahn, C., Torres, O., Abdullaev, S., Limbacher, J., and Kahn, R. A.: Analysis of a saline dust storm from the Aralkum Desert – Part 1: Consistency between multisensor satellite aerosol products, Atmos. Chem. Phys., 25, 7403-7429, https://doi.org/10.5194/acp-25-7403-2025, 2025.

Yang, A., Tan, Q., Rajapakshe, C., Chin, M., and Yu, H.: Global premature mortality by dust and pollution PM2.5 estimated from aerosol reanalysis of the modern-era retrospective analysis for research and applications, version 2, Frontiers in Environmental Science, Volume 10 - 2022, https://doi.org/10.3389/fenvs.2022.975755, 2022.

Yu, H., Chin, M., Remer, L. A., Kleidman, R. G., Bellouin, N., Bian, H., and Diehl, T.: Variability of marine aerosol fine-mode fraction and estimates of anthropogenic aerosol component over cloud-free oceans from the Moderate Resolution Imaging Spectroradiometer (MODIS), J Geophys Res Atmospheres, 114, https://doi.org/10.1029/2008JD010648, 2009.

Yu, H., Remer, L. A., Chin, M., Bian, H., Tan, Q., Yuan, T., and Zhang, Y.: Aerosols from overseas rival domestic emissions over North America, Science, 337, 566–569, https://doi.org/10.1126/science.1217576, 2012.

Yu, H., Chin, M., Bian, H., Yuan, T., Prospero, J. M., Omar, A. H., Remer, L. A., Winker, D. M., Yang, Y., and Zhang, Y.: Quantification of trans-Atlantic dust transport from seven-year (2007–2013) record of CALIPSO lidar measurements, Remote Sens Environ, 159, 232-249, 2015a.

Yu H., M. Chin, T. L. Yuan, H. Bian, L. A. Remer, J. M. Prospero, A. Omar, D. Winker, Y. Yang, Y. Zhang, Z. Zhang and C. Zhao. The fertilizing role of African dust in the Amazon rainforest: A first multiyear assessment based on data from Cloud-Aerosol Lidar and Infrared Pathfinder Satellite Observations., Geophysical Research Letters, 42 (6): 1984-1991 [10.1002/2015GL063040], 2015b.

Yu, H., Yang, Y., Wang, H., Tan, Q., Chin, M., Levy, R. C., Remer, L. A., Smith, S. J., Yuan, T., and Shi, Y.: Interannual variability and trends of combustion aerosol and dust in major continental outflows revealed by MODIS retrievals and CAM5 simulations during 2003–2017, Atmospheric Chemistry and Physics, *Atmospheric Chemistry and Physics,* 20 139-161 [10.5194/acp-20-139-2020] 2020.

Yu, H., Tan, Q., Chin, M., Remer, L. A., Kahn, R. A., Bian, H., Kim, D., Zhang, Z., Yuan, T., Omar, A. H., Winker, D. M., Levy, R. C., Kalashnikova, O., Crepeau, L., Capelle, V., and Chédin, A.: Estimates of African Dust Deposition Along the Trans-Atlantic Transit Using the Decadelong Record of Aerosol Measurements from CALIOP, MODIS, MISR, and IASI, J Geophys Res Atmospheres, 124, 7975-7996, https://doi.org/10.1029/2019JD030574, 2019.

Zender, C. S., Bian, H., and Newman, D.: Mineral Dust Entrainment and Deposition (DEAD) model: Description and 1990s dust climatology, J Geophys Res Atmospheres, 108,

https://doi.org/10.5194/egusphere-2026-4322
Preprint. Discussion started: 17 August 2026

https://doi.org/10.1029/2002JD002775, 2003.

Zhang, H., McFarquhar, G. M., Saleeby, S. M., and Cotton, W. R.: Impacts of Saharan dust as CCN on the evolution of an idealized tropical cyclone, Geophys Res Lett, 34, 2007.

Zhang, H., Zhao, S., Wang, Z., Zhang, X., and Song, L.: The updated effective radiative forcing of major anthropogenic aerosols and their effects on global climate at present and in the future, International Journal of Climatology, 36, 4029-4044, https://doi.org/10.1002/joc.4613, 2016.

Zhang, X., Li, L., Chen, C., Derimian, Y., Dubovik, O., Lopatin, A., Fuertes, D., Holben, B., and Sinyuk, A.: Aerosol Components Derived from Global AERONET Measurements by GRASP: A New Value-Added Aerosol Component Global Dataset and Its Application, Bull. Amer. Meteor. Soc., 105, E1822–E1848, https://doi.org/10.1175/BAMS-D-23-0260.1, 2024.

Zhao, A., Ryder, C. L., and Wilcox, L. J.: How well do the CMIP6 models simulate dust aerosols?, Atmos. Chem. Phys., 22, 2095-2119, https://doi.org/10.5194/acp-22-2095-2022, 2022.

Zhao, M., Golaz, J.-C., Held, I. M., Guo, H., Balaji, V., Benson, R., Chen, J.-H., Chen, X., Donner, L. J., Dunne, J. P., Dunne, K., Durachta, J., Fan, S.-M., Freidenreich, S. M., Garner, S. T., Ginoux, P., Harris, L. M., Horowitz, L. W., Krasting, J. P., Langenhorst, A. R., Liang, Z., Lin, P., Lin, S.-J., Malyshev, S. L., Mason, E., Milly, P. C. D., Ming, Y., Naik, V., Paulot, F., Paynter, D., Phillipps, P., Radhakrishnan, A., Ramaswamy, V., Robinson, T., Schwarzkopf, D., Seman, C. J., Shevliakova, E., Shen, Z., Shin, H., Silvers, L. G., Wilson, J. R., Winton, M., Wittenberg, A. T., Wyman, B., and Xiang, B.: The GFDL Global Atmosphere and Land Model AM4.0/LM4.0: 1. Simulation Characteristics With Prescribed SSTs, Journal of Advances in Modeling Earth Systems, 10, 691-734, https://doi.org/10.1002/2017MS001208, 2018.

Zhao, S., Zhang, H., Feng, S., and Fu, Q.: Simulating direct effects of dust aerosol on arid and semi-arid regions using an aerosol-climate coupled system, Int. J. Climatol, 35, 1858-1866, 2015.

Zheng, J., Yu, H., Zhou, Y., Shi, Y., Zhang, Z., Di Biagio, C., Formenti, P., and Smirnov, A.: A novel retrieval of global dust optical depth and effective diameter based on MODIS thermal infrared observations, Remote Sens Environ, 332, 115083, https://doi.org/10.1016/j.rse.2025.115083, 2026.

Zheng, J., Zhang, Z., DeSouza-Machado, S., Ryder, C. L., Garnier, A., Di Biagio, C., Yang, P., Welton, E. J., Yu, H., and Barreto, A.: Assessment of dust size retrievals based on AERONET: A case study of radiative closure from visible-near-infrared to thermal infrared, Geophys Res Lett, 51, e2023GL106808, 2024.

Zheng, J., Zhang, Z., Garnier, A., Yu, H., Song, Q., Wang, C., Dubuisson, P., and Di Biagio, C.: The thermal infrared optical depth of mineral dust retrieved from integrated CALIOP and IIR observations, Remote Sens Environ, 270, 112841, https://doi.org/10.1016/j.rse.2021.112841, 2022.

Zheng, J., Zhang, Z., Yu, H., Garnier, A., Song, Q., Wang, C., Di Biagio, C., Kok, J. F., Derimian, Y., and Ryder, C.: Thermal infrared dust optical depth and coarse-mode effective diameter over oceans retrieved from collocated MODIS and CALIOP observations, Atmos. Chem. Phys., 23, 8271-8304, https://doi.org/10.5194/acp-23-8271-2023, 2023.

Zhou, C. H., Gong, S. L., Zhang, X. Y., Liu, H. L., Xue, M., Cao, G. L., An, X. Q., Che, H. Z., Zhang, Y. M., and Niu, T.: Towards the improvements of simulating the chemical and optical properties of Chinese aerosols using an online coupled model – CUACE/Aero, Tellus B, 64,

https://doi.org/10.5194/egusphere-2026-4322
Preprint. Discussion started: 17 August 2026

18965, https://doi.org/10.3402/tellusb.v64i0.18965, 2012.

Zuidema, P., Alvarez, C., Kramer, S. J., Custals, L., Izaguirre, M., Sealy, P., Prospero, J. M., and Blades, E.: Is Summer African Dust Arriving Earlier to Barbados? The Updated Long-Term In Situ Dust Mass Concentration Time Series from Ragged Point, Barbados, and Miami, Florida, B Am Meteorol Soc, 100, 1981-1986, https://doi.org/10.1175/BAMS-D-18-0083.1, 2019.